4D-Var inversion of European NH3 emissions using CrIS NH3 measurements and GEOS-Chem adjoint with bi-directional and uni-directional flux schemes

Hansen Cao[1], Daven K. Henze[1], Liye Zhu[2], Mark W Shephard[3], Karen Cady-Pereira[4], Enrico Dammers[5], Michael Sitwell[5], Nicholas Heath[6], Chantelle Lonsdale[7], Jesse Owen Bash[8], Kazuyuki Miyazaki[9], Chris Flechard[10], Yannick Fauvel[11], Roy J. Wichink Kruit[12], Stefan Feigenspan[13], Christian Brümmer[14], Frederik Schrader[14], Marsailidh Twigg[15], sarah Leeson[16], Yuk Sim Tang[17], Amy C.M. Stephens[17], Christine Braban[18], Keith Vincent[19], Mario Meier[20], Eva Seitler[20], Camilla Geels[21], Thomas Ellermann[21], Agnieszka Sanocka[19], and Shannon L Capps[22]

[1]University of Colorado Boulder
[2]Sun Yat-sen University
[3]Environment Canada
[4]Atmospheric and Environmental Research, Inc.
[5]Environment and Climate Change Canada
[6]Atmospheric and Environmental Research Inc., USA
[7]Department of Civil, Structural and Environmental Engineering, University at Buffalo
[8]U.S. EPA
[9]Jet Propulsion Laboratory
[10]INRAE (National Research Institute for Agriculture, Food and Environment), UMR SAS, Agrocampus Quest
[11]INRAE
[12]National Institute for Public Health and the Environment
[13]German Environment Agency
[14]Thünen Institute of Climate-Smart Agriculture
[15]UK Centre for Ecology & Hydrology, Bush Estate, Penicuik
[16]Centre of Ecology and Hydrology (CEH)
[17]Centre for Ecology and Hydrology
[18]Center for Ecology and Hydrology
[19]Ricardo Energy & Environment
[20]Forschungsstelle fur Umweltbeobachtung
[21]Aarhus University
[22]Georgia Institute of Technology

November 22, 2022

Abstract

We conduct the first 4D-Var inversion of NH3 accounting for NH3 bidirectional flux, using CrIS satellite NH3 observations

over Europe in 2016. We find posterior NH3 emissions peak more in springtime than prior emissions at continental to national scales, and annually they are generally smaller than the prior emissions over central Europe, but larger over most of the rest of Europe. Annual posterior anthropogenic NH3 emissions for 25 European Union members (EU25) are 25% higher than the prior emissions and very close(<2% difference) to other inventories. Our posterior annual anthropogenic emissions for EU25, the UK, the Netherlands, and Switzerland are generally 10-20% smaller than when treating NH3 fluxes as uni-directional emissions, while the monthly regional difference can be up to 34% (Switzerland in July). Compared to monthly mean in-situ observations, our posterior NH3 emissions from both schemes generally improve the magnitude and seasonality of simulated surface NH3 and bulk NHx wet deposition throughout most of Europe, whereas evaluation against hourly measurements at a background site shows the bi-directional scheme better captures observed diurnal variability of surface NH3. This contrast highlights the need for accurately simulating diurnal variability of NH3 in assimilation of sun-synchronous observations and also the potential value of future geostationary satellite observations. Overall, our top-down ammonia emissions can help to examine the effectiveness of air pollution control policies to facilitate future air pollution management, as well as helping us understand the uncertainty in top-downNH3emission estimates associated with treatment of NH3surface exchange.

4D-Var inversion of European NH$_3$ emissions using CrIS NH$_3$ measurements and GEOS-Chem adjoint with bi-directional and uni-directional flux schemes

Hansen Cao[1], Daven K. Henze[1], Liye Zhu[2], Mark W. Shephard[3], Karen Cady-Pereira[4], Enrico Dammers[5], Michael Sitwell[3], Nicholas Heath[4], Chantelle Lonsdale[6], Jesse O. Bash[7], Kazuyuki Miyazaki [8], Christophe Flechard[9], Yannick Fauvel[9], Roy Wichink Kruit[10], Stefan Feigenspan[11], Christian Brümmer[12], Frederik Schrader[12], Marsailidh M. Twigg[13], Sarah Leeson[13], Yuk S. Tang[13], Amy C.M. Stephens[13], Christine Braban[13], Keith Vincent[14], Mario Meier[15], Eva Seitler[15], Camilla Geels[16], Thomas Ellermann[16], Agnieszka Sanocka[14], Shannon L. Capps[17]

[1]University of Colorado, Boulder, USA

[2]Sun Yat-sen University, China

[3]Environment and Climate Change Canada, Toronto, Ontario, Canada

[4]Atmospheric and Environmental Research Inc., USA

[5]Netherlands Organisation for Applied Scientific Research (TNO), Climate Air and Sustainability (CAS),

Utrecht, The Netherlands

[6]Department of Civil, Structural and Environmental Engineering, University at Buffalo, Buffalo, NY USA

[7]U.S. Environmental Protection Agency, USA

[8]Jet Propulsion Laboratory, California Institute of Technology, USA

[9]INRAE (National Research Institute for Agriculture, Food and Environment), UMR SAS, Agrocampus

Ouest, 65 rue de Saint-Brieuc, 35042 Rennes, France

[10]National Institute for Public Health and the Environment, The Netherlands

[11]German Environment Agency, Germany

[12]Thünen Institute of Climate-Smart Agriculture, Germany

[13]UK Centre for Ecology & Hydrology, UK

[14]Ricardo Energy & Environment, Wantage, England, UK

[15]Forschungsstelle für Umweltbeobachtung, Switzerland

[16]Department of Environmental Science, Aarhus University, Denmark

[17]Civil, Architectural, and Environmental Engineering Department, Drexel University, Philadelphia, PA,

USA

Corresponding author: Daven K. Henze, `daven.henze@colorado.edu`

Key Points:

- First 4D-Var inversion to include bi-directional flux of NH_3, based on CrIS NH_3 and cross-validated with surface observations.

- Bi-directional flux reduces posterior regional NH_3 emissions by 10-20% annually (monthly up to 34%), compared to uni-directional emissions.

- Posterior NH_3 emissions generally improve simulated seasonality and magnitude of NH_3 and NH_x wet deposition.

Abstract

We conduct the first 4D-Var inversion of NH_3 accounting for NH_3 bidirectional flux, using CrIS satellite NH_3 observations over Europe in 2016. We find posterior NH_3 emissions peak more in springtime than prior emissions at continental to national scales, and annually they are generally smaller than the prior emissions over central Europe, but larger over most of the rest of Europe. Annual posterior anthropogenic NH_3 emissions for 25 European Union members (EU25) are 25% higher than the prior emissions and very close ($< 2\%$ difference) to other inventories. Our posterior annual anthropogenic emissions for EU25, the UK, the Netherlands, and Switzerland are generally 10-20% smaller than when treating NH_3 fluxes as uni-directional emissions, while the monthly regional difference can be up to 34% (Switzerland in July). Compared to monthly mean in-situ observations, our posterior NH_3 emissions from both schemes generally improve the magnitude and seasonality of simulated surface NH_3 and bulk NH_x wet deposition throughout most of Europe, whereas evaluation against hourly measurements at a background site shows the bi-directional scheme better captures observed diurnal variability of surface NH_3. This contrast highlights the need for accurately simulating diurnal variability of NH_3 in assimilation of sun-synchronous observations and also the potential value of future geostationary satellite observations. Overall, our top-down ammonia emissions can help to examine the effectiveness of air pollution control policies to facilitate future air pollution management, as well as helping us understand the uncertainty in top-down NH_3 emission estimates associated with treatment of NH_3 surface exchange.

Plain Language Summary

Atmospheric ammonia contributes to air pollutants and excessive deposition of reactive nitrogen that is detrimental to sensitive ecosystems. Ammonia is emitted mainly by agricultural livestock and fertilizer use. While surface measurements of NH_3 are sparse, satellite observations can provide near daily global coverage. Here we calculate monthly NH_3 emissions over Europe, the only region adopting NH_3 control policies, using an air quality model coupled with a process-based bi-directional NH_3 flux scheme and NH_3 measurements observed by the CrIS satellite instrument. Our CrIS-derived annual regional total anthropogenic NH_3 emissions are close ($< 2\%$ difference) to statistic-based bottom-up estimates and are 10-20% lower than when treating NH_3 exchange between the atmosphere and biosphere as one-way emissions. Our top-down NH_3 emission estimates

71 may help to assess the efficacy of NH_3 abatement policies and provide quantitative sup-

72 port for future policy making.

1 Introduction

74   Atmospheric ammonia (NH_3) has adverse effects on human health, ecosystem sta-

75 bility and climate change via formation of fine particulate matter ($PM_{2.5}$) and excessive

76 deposition of reactive nitrogen (Nr) to bodies of water (Krupa, 2003; Myhre et al., 2009;

77 Behera et al., 2013; J. W. Erisman et al., 2013; Nah et al., 2018; Sutton et al., 2020).

78 Ammonia and ammonium (collectively, NH_x) also modulate soil pH through deposition

79 to surface soil (Galloway et al., 2003; Krupa, 2003). Ammonia is emitted mainly from

80 agricultural activities ($> 80\%$) at national and global scales (EEA, 2017; U.S. EPA, 2018;

81 Huang et al., 2012; McDuffie et al., 2020; Crippa et al., 2020) but can be dominated by

82 non-agricultural emissions at local scales (Chang et al., 2016; Fenn et al., 2018; Berner

83 & Felix, 2020). NH_3 emissions have been reported to pose severe air pollution problems

84 and contribute to premature death across the world (Lelieveld et al., 2015). Surface mea-

85 surements of ambient and precipitation concentrations across Europe and the US also

86 show that NH_x is becoming the dominant contributor to Nr pollution given the substan-

87 tial reduction of SO_x and NO_x emissions over the past decades (Tang et al., 2021; Du

88 et al., 2014; Ellis et al., 2013; Li et al., 2016; Sutton et al., 2020; Elguindi et al., 2020).

89 With sustained decreasing trends in SO_x and NO_x emissions projected alongside increas-

90 ing trends in NH_3 emissions, NH_x pollution is expected to become worse during the next

91 few years. On top of that, it has been shown that there is a climate penalty on ammo-

92 nia, resulting in increased emissions in a warmer future climate (Skjøth & Geels, 2013).

93 Some studies have shown that reducing ammonia emissions is a cost-effective way to mit-

94 igate $PM_{2.5}$ pollution and nitrogen deposition (J. Erisman & Schaap, 2004; Paulot et

95 al., 2014; X. Zhang et al., 2020). More specifically, recent studies show that reducing agri-

96 cultural NH_3 emissions through changing livestock diets and improving animal housing

97 as well as covering manure storage and fertilizer application are feasible and cost-effective

98 ways to mitigate NH_x air pollution in Europe, the US and China (Giannakis, Kushta,

99 Giannadaki, et al., 2019; Goodkind et al., 2019; X. Zhang et al., 2020). Wetland restora-

100 tion may also be a cost-effective way to reduce nitrogen pollution through biogeochem-

101 ical process-based nutrient removal (Cheng et al., 2020). Reducing NH_x pollution there-

102 fore has become an urgent need and an achievable goal for many countries, especially

103 for some European countries facing the threat of a severe "nitrogen crisis" (Stokstad, 2019).

104 Since 1991, Europe has implemented a series of NH_3 abatement policies and achieved

105 a 25% decrease in NH_3 emissions from 1990 to 2010 (EEA, 2017; Giannakis, Kushta, Brugge-

106 man, & Lelieveld, 2019; UNECE, 1999), primarily due to reductions in livestock emis-

107 sions. However, more than 93% of NH_3 emissions over Europe in 2013 are still from agri-

108 cultural sources (EEA, 2017). Therefore, additional efforts have been made to reduce

109 NH_3 emissions over Europe during the past decade. For instance, a recent version of Gothen-

110 burg Protocol amended in 2012 has set a decreasing emission ceiling for European coun-

111 tries for 2005 to 2020, that aims to reduce NH_3 emissions to 3.624 Tg y^{-1} in 2020 (EEA,

112 2020); however, bottom-up emission estimates still show a slight increase (0.6% y^{-1}) from

113 2010 to 2018 (EEA, 2020; McDuffie et al., 2020), mostly due to increasing agricultural

114 activities.

115 To better understand and mitigate the environmental effects of NH_3 and to exam-

116 ine the efficacy of NH_3 abatement policies as well as to facilitate future policy-making,

117 long-term and up-to-date ammonia emission monitoring with high accuracy and fine res-

118 olution as well as great spatial coverage is required. Although bottom-up inventories are

119 able to capture the general spatial pattern and trends in activity data to some degree,

120 they typically have large uncertainties due to uncertain emission factors and missing po-

121 tential sources over areas with limited statistics. Furthermore, they are unlikely to ac-

122 count for the climate-driven or meteorology-driven change (e.g., temperature and wind

123 speed) in emission factors and activity increases in small-scale sources (McDuffie et al.,

124 2020; Hoesly et al., 2018; Sommer et al., 2019; Sutton et al., 2013; Bash et al., 2013).

125 Meanwhile, direct ammonia emission monitoring is usually expensive and thus is not fea-

126 sible to be carried out at large scales. Instead, monitoring NH_3 concentrations and its

127 downstream products (e.g., NH_4^+ and NH_x wet deposition) at relatively lower cost can

128 be used to investigate NH_3 emissions from local to national scales and to help assess the

129 effectiveness of emission control policies (Sutton et al., 2003; Nair & Yu, 2020).

130 Previous studies have used ground-based measurements of NH_x concentrations and

131 NH_x wet deposition to explore and constrain the seasonal cycle, interannual variability,

132 and magnitude of ammonia emissions at local to regional scales around the world (Sutton

133 et al., 2003; Gilliland et al., 2003; Pinder et al., 2006; Henze et al., 2009; L. Zhang et al.,

2012; Paulot et al., 2014; Tang, Braban, et al., 2018; Lonati & Cernuschi, 2020; Kong et al., 2019). The limitations of these surface measurement-based approaches lie in the scarcity of surface monitoring sites and uncertainty and biases in the instruments (von Bobrutzki et al., 2010).

Alternatively, satellite NH_3 observations can be used to monitor NH_3 emissions. In terms of spatial coverage and long-term trends, satellite observations of NH_3 offer distinct advantages over surface NH_x observations. Space-based observations of NH_3 have thus been leveraged to study and constrain the spatiotemporal variation and magnitude of NH_3 emissions and model simulations of NH_x during the past decade (Zhu et al., 2013; Schiferl et al., 2016; Warner et al., 2016, 2017; L. Zhang et al., 2018; Van Damme et al., 2018; Dammers et al., 2019; Clarisse, Van Damme, Clerbaux, & Coheur, 2019; Clarisse, Van Damme, Gardner, et al., 2019; Cao et al., 2020; Chen et al., 2021; Van Damme et al., 2020; R. Wang et al., 2021; Evangeliou et al., 2021; Marais et al., 2021). Atmospheric NH_3 concentrations can be retrieved from measured infrared radiance by remote sensing instruments onboard multiple satellites, such as Atmospheric Infrared Sounder (AIRS) onboard NASA's Aqua satellite (Warner et al., 2016), Tropospheric Emission Spectrometer (TES) onboard NASA's Aura satellite (Beer et al., 2008; Shephard et al., 2011), Infrared Atmospheric Sounding Interferometer (IASI) onboard European Space Agency's MetOp satellites (Clarisse et al., 2009; Van Damme et al., 2014), and Cross-track Infrared Sounder (CrIS) onboard NOAA's Suomi-NPP satellite (Shephard & Cady-Pereira, 2015; Shephard et al., 2020) and NOAA-20 satellite (Glumb et al., 2018). Schiferl et al. (2016) used summertime morning IASI NH_3 column observations along with the GEOS-Chem model simulations and AMoN surface NH_3 measurements to explore the drivers of annual variability of NH_3 concentrations. Van Damme et al. (2018), Clarisse et al. (2019) and Dammers et al. (2019) used IASI-observed and CrIS-observed NH_3 column concentrations to quantify NH_3 emissions from large point sources through an oversampling approach. Warner et al. (2016) and Wang et al. (2021) analyzed spatial and intra-annual variability in AIRS and IASI observations at regional and global scales to identify major sources of NH_3 in different regions during different seasons. Warner et al. (2017) and van Damme et al. (2020) explored the interannual variability in long-term global NH_3 observations from AIRS and IASI instruments and found a general increasing trend in atmospheric NH_3 over China, Europe and the US from 2002 to 2018. Along with chemical transport models and their adjoint models, Zhu et al. (2013), L. Zhang et al. (2018),

Cao et al. (2020) and Chen et al. (2021) applied TES and CrIS NH_3 profiles and IASI NH_3 column concentrations for inverse modeling of NH_3 emissions and generally found significant heterogeneous biases in anthropogenic NH_3 inventories across the US and China. Most recently, Marais et al. (2021) used the GEOS-Chem forward model and multiyear (2013-2018) NH_3 column concentrations from IASI and CrIS to constrain spatiotemporal variation and magnitude of NH_3 emissions in the UK, and they found that bottom-up inventories were biased low by 27-49% and miss the summer emissions peak compared to satellite-derived NH_3 emissions.

Most previous inverse modeling studies (Henze et al., 2009; Zhu et al., 2013; Paulot et al., 2014; L. Zhang et al., 2018; Cao et al., 2020; Chen et al., 2021) using either satellite observations or surface observations have only used uni-directional (uni-di) dry deposition scheme (Wesely, 1989), which treats surface exchange of NH_3 between the atmosphere and biosphere in a one-way manner (from air to surface) and ignores the impacts of change in environmental conditions (e.g., soil temperature, soil wetness, soil pH, fertilized condition and vegetation type) on NH_3 emissions from fertilized soil and crops, which likely lead to high biases in top-down NH_3 emission estimates. However, early studies have found that a process-based bi-directional (bi-di) NH_3 flux scheme (Sutton et al., 1998) involving environmental conditions more realistically captures the dynamics in measured net NH_3 fluxes in Europe and North America (Sutton et al., 1998; Nemitz et al., 2001; Neirynck & Ceulemans, 2008; Pleim et al., 2013). Later, application of bi-di NH_3 flux schemes in regional and global chemical transport models generally enabled better model performance in representing ground-based and space-based measurements of NH_3 surface and column concentrations and NH_x wet depositions over Europe and North America as well as East Asia (Wichink Kruit et al., 2012; Bash et al., 2013; Zhu, Henze, Bash, Jeong, et al., 2015; Pleim et al., 2019).

Therefore, to derive NH_3 emissions from satellite observations while accounting for spatial and temporal changes in environmental conditions, use of a chemical transport model with a process-based bi-di NH_3 flux scheme is preferable (Sutton et al., 2013). In addition, since Sun-synchronous satellites measure atmospheric NH_3 concentrations only at certain time (e.g., the daytime and nighttime overpass of CrIS is around 13:30 LT and 01:30 LT, respectively), accurately simulating the diurnal variability of NH_3 can increase the accuracy of top-down emission estimates (Zhu, Henze, Bash, Cady-Pereira, et al., 2015). Recently, van der Graaf et al. (2021) included a bi-di NH_3 flux scheme when as-

similating CrIS-NH3 observations to improve the spatiotemporal NH_3 distribution in Europe. Here we aim to conduct the first side-by-side comparison of an NH_3 inversion using both uni-directional and bi-di NH_3 flux schemes.

Based on a more complex bi-di NH_3 flux scheme in the CMAQ model (Bash et al., 2013), Zhu, Henze, Bash, Jeong, et al. (2015) implemented a simplified bi-di NH_3 flux scheme in the GEOS-Chem model involving soil temperature, soil pH, soil wetness, soil NH_4^+ concentrations and vegetation type and first developed the corresponding adjoint processes for this bi-di NH_3 flux scheme. With this updated GEOS-Chem forward and adjoint model, they first investigated the spatial and temporal sensitivity of simulated NH_3 concentration to fertilizer application rate and to soil pH at the global scale.

Here we incorporate the bi-di forward and bi-di adjoint processes developed by Zhu, Henze, Bash, Jeong, et al. (2015) into a more recent GEOS-Chem adjoint model version (v35m) coupled with the CrIS NH_3 observation operator (Cao et al., 2020) and apply this updated GEOS-Chem adjoint model to constraining NH_3 emissions using CrIS daytime NH_3 profile observations in 2016 using the four dimensional variational (4D-Var) approach. To more completely understand the implications of neglecting the bi-di exchange of NH_3 (as all previous top-down studies have done), we also conduct a 4D-Var inversion using uni-di NH_3 emissions and compare our posterior NH_3 emissions from these two inversions, presenting the first side-by-side study to explore the uncertainty in top-down NH_3 emission estimates arising from the NH_3 flux scheme. We use CrIS NH_3 because 1) it provides vertical profiles and averaging kernels (essential for data assimilation), both which are absent from IASI retrievals, and 2) it combines extensive spatial coverage, low noise and fine spatial resolution (Shephard & Cady-Pereira, 2015), and 3) it has greater spatial coverage than TES, with global coverage similar to IASI and AIRS, and lower signal noise compared to other sensors (Zavyalov et al., 2013), which improves sensitivity in the boundary layer. We further evaluate our CrIS-derived NH_3 emission estimates using independent measurements of surface NH_3 and bulk wet NH_x deposition from domain-wide monitoring sites over Europe in 2016.

2 Data

2.1 CrIS NH$_3$ observations

CrIS is an infrared sounder on board the sun-synchronous satellite Suomi National Polar-orbiting Partnership (SNPP, used here) (Tobin, 2012) launched in October 2011 and the NOAA-20 (JPSS-1) launched in November 2017 (Glumb et al., 2018). CrIS has a cross-track scanning swath width of 2200 km and a nadir spatial resolution of 14 km, which enable CrIS to achieves global coverage twice a day with daytime and nighttime overpasses at 13:30 local time (LT) and 01:30 LT, respectively. NH$_3$ profile and column observations are retrieved through the CrIS Fast Physical Retrieval algorithm (CFPR), which minimizes the difference between measured and simulated spectral radiance in the NH$_3$ spectral feature around 967 cm^{-1} (Shephard & Cady-Pereira, 2015). Pixel-specific a priori profiles and averaging kernels comprise the observation operator ($\boldsymbol{H}$), which is essential for comparison between satellite retrievals and model simulations. The CFPR algorithm uses three a priori NH$_3$ profiles, representative of polluted, moderately polluted, and clear conditions. For each NH$_3$ retrieval, one a priori profile is selected based on an estimated NH$_3$ signal (Shephard & Cady-Pereira, 2015). We used high-quality daytime CrIS v1.5 NH$_3$ observations (QF $\geq$ 3) (Shephard et al., 2020) over the Europe domain [15ºW-40ºE, 32º-62ºN] in 2016. Daytime CrIS NH$_3$ observations have been validated by and generally show good agreement with ground-based and aircraft observations in select regions (Shephard & Cady-Pereira, 2015; Dammers et al., 2017).

We derived linearized averaging kernels ($\frac{\partial(\boldsymbol{x_{retrieval}})}{\partial(\boldsymbol{x_{true}})}$) from the original logarithmic averaging kernels ($\frac{\partial(ln(\boldsymbol{x_{retrieval}}))}{\partial(ln(\boldsymbol{x_{true}}))}$) following L. Zhang et al. (2010) and Cao et al. (2020) to avoid 1) unrealistic small model column concentrations with the application of logarithmic averaging kernels and 2) numerically large gradient of the cost function with respect to simulated NH$_3$ concentrations in our 4D-Var inversion. $\boldsymbol{x_{retrieval}}$ and $\boldsymbol{x_{true}}$ are CrIS NH$_3$ profile retrieval and the true state of atmospheric NH$_3$ profile, respectively. During the lineariztion of the averaging kernels (L. Zhang et al., 2010), we also limited the ratio of $\frac{\boldsymbol{x_a}(i)}{\boldsymbol{x_a}(j)}$ to be in the range of 0 to 3 in order to avoid unrealistically large values of averaging kernels at higher levels. $\boldsymbol{x_a}(i)$ and $\boldsymbol{x_a}(j)$ are CrIS NH$_3$ a priori at level i and j, respectively.

Figures 1 (a)-(d) show the spatial and seasonal variability of CrIS NH$_3$ mixing ratios at surface level over Europe for March, June, September and December 2016. Higher

260 NH$_3$ concentrations are generally found during warm months over northern Germany,

261 the Netherlands, western France, Northern Italy, South UK and Ireland as well as south-

262 ern and northeastern Spain, where there are intense agricultural activities. Unlike the

263 US (Cao et al., 2020), Europe saw higher CrIS NH$_3$ concentrations in September than

264 in June, which is consistent with the September/June contrast in independent surface

265 measurements of NH$_3$ averaged across the European domain (Fig. 10 (a)). This Septem-

266 ber/June contrast in both space-based and ground-based surface NH$_3$ observations is most

267 likely caused by larger NH$_x$ wet deposition in June than in September (Fig. 11 (a)), but

268 this might not represent the typical condition of a normal year since 2016 was exception-

269 ally warm across Europe (`https://www.knmi.nl/nederland-nu/klimatologie/maand`

270 `-en-seizoensoverzichten/2016/jaar`).

2.2 Surface observations

272 We evaluate CrIS-derived NH$_3$ emissions using extensive independent measurements

273 of surface NH$_3$ and bulk NH$_x$ wet deposition in 2016 collected from the European Mon-

274 itoring and Evaluation Programme (EMEP) (Tørseth et al., 2012), the UK Eutrophy-

275 ing and Acidifying Atmospheric Pollutants (UKEAP) networks: National Ammonia Mon-

276 itoring Network (NAMN, `https://uk-air.defra.gov.uk/interactive-map?network=`

277 `namn`) (Tang, Stephens, et al., 2018), the Measuring Ammonia in Nature (MAN) network

278 (Lolkema et al., 2015) and the Dutch Monitoring Air Quality Network (LML; Landelijk

279 Meetnet Luchtkwaliteit) (van Zanten et al., 2017) in the Netherlands, a nation-wide am-

280 monia monitoring network in Switzerland (Seitler & Meier, 2021), the German Länder

281 networks and the German Environment Agency (`https://www.umweltbundesamt.de`),

282 the Danish Background Air Quality Monitoring Program (Ellermann et al., 2018; Geels

283 et al., 2012), as well as some short-term field campaign sites and long-term monitoring

284 sites distributed in France (Flechard et al., 2011), Germany (Wintjen et al., 2020; Zöll

285 et al., 2016, 2019), and UK (Twigg et al., 2015; H. L. Walker et al., 2019).

3 Methods

3.1 Uni-di and bi-di NH$_3$ flux schemes

288 Both uni-di and bi-di NH$_3$ flux schemes are treated like an electrical resistance model,

289 wherein the flux between the atmosphere and biosphere is analogous to electrical cur-

rent and the difference between the air and surface concentrations is analogous to electrical voltage (Wesely, 1989). While the uni-di scheme assumes the surface concentration to be zero and thus the air-surface exchange is only downward deposition from the atmosphere to the biosphere (Wesely, 1989), the bi-di scheme more realistically accounts for both air-to-surface deposition and surface-to-air diffusion by introducing a canopy compensation point. This approach, while recognized for some time, has been increasingly implemented in regional and global CTMs in recent years (Sutton et al., 1998; Nemitz et al., 2001; Wichink Kruit et al., 2012; Bash et al., 2013; Pleim et al., 2013; J. T. Walker et al., 2013; Zhu, Henze, Bash, Jeong, et al., 2015; Pleim et al., 2019). A key aspect of the bi-di scheme is the calculation of the canopy compensation point (C_c), which involves the resistances in the quasi-laminar boundary layers of leaf surface and ground surface, resistances in the leaf stomatal and cuticle and soil, and NH_3 emission potential in the soil and stomatal, as well as soil temperature and leaf surface temperature (Zhu, Henze, Bash, Jeong, et al., 2015). The direction of bi-di NH_3 flux is determined by the sign of the difference between the canopy compensation point and ambient NH_3 concentration (C_c - C_a). NH_3 emission potential in the soil is calculated as the ratio of soil NH_4^+ concentration to soil H^+ concentration. The sources of soil NH_4^+ include fertilizer application and wet and dry deposition. Only 60% of the deposited NH_4^+ is assumed to enter the soil, while the rest is assumed to being lost due to run-off into waterways (Hudman et al., 2012). The major sink of soil NH_4^+ is nitrification with a lifetime of 15 days (Zhu, Henze, Bash, Jeong, et al., 2015).

3.2 GEOS-Chem and its adjoint model

We use GEOS-Chem v9-02 with a bi-di NH_3 flux scheme (Zhu, Henze, Bash, Jeong, et al., 2015) to relate NH_3 emissions to NH_3 concentrations in the atmosphere. The corresponding adjoint model (v35m) is used to derive the gradient of the cost function with respect to NH_3 emissions and fertilizer rates in our 4D-Var inversion. Our GEOS-Chem nested simulations were driven by Goddard Earth Observing System (GEOS-FP) assimilated meteorological fields with a horizontal resolution of 0.25° latitude × 0.3125° longitude and 47 vertical levels up to 0.01 hPa over the Europe domain ([15°W-40°E, 32°-62°N]). The boundary conditions from global simulations with a horizontal resolution of 2° latitude × 2.5° longitude were supplied to our nested simulations every 3 hours.

321   In order to reduce computation cost, we use an offline NH_x simulation in our 4D-

322 Var inversion following previous studies (Paulot et al., 2014; L. Zhang et al., 2018; Cao

323 et al., 2020). We only simulate NH_3 emissions, wet and dry deposition (H. Liu et al., 2001;

324 Q. Wang et al., 2011; Amos et al., 2012; Wesely, 1989; Y. Wang et al., 1998; L. Zhang

325 et al., 2001), transport of NH_x, and NH_x partitioning (Binkowski & Roselle, 2003; Park

326 et al., 2004) in our offline simulations. The NH_x partitioning is driven by archived hourly

327 SO_4^{2-}, HNO_3, and NO_3^- concentrations from the standard O_3-NO_x-VOC-aerosol simu-

328 lation (Park et al., 2004; Mao et al., 2010). The high-biased GEOS-Chem-simulated HNO_3

329 (L. Zhang et al., 2012; Heald et al., 2012) was reduced by 15% at each time step (10 min-

330 utes) before the NH_3-NH_4^+ partitioning in the aerosol thermodynamics following Heald

331 et al. (2012).

332   Changes in emissions of SO_x and NO_x can modulate the lifetime of NH_3 in the at-

333 mosphere (M. Liu et al., 2018; Yu et al., 2018). Here we drive our standard simulations,

334 which were used to output hourly SO_4^{2-}, NO_3^- and HNO_3 at 0.3125^o longitude $\times$ 0.25^o

335 latitude for the year 2016, using rescaled SO_x and NO_x emissions from HTAP v2 (orig-

336 inally for 2010) by emission reduction ratio taken from satellite-derived SO_2 and NO_x

337 emissions (Miyazaki et al., 2019, 2020).

338   Our prior NH_3 emissions consist of livestock emissions from HTAP v2 (Janssens-

339 Maenhout et al., 2015), emissions originating from fertilizer application (Lu & Tian, 2017)

340 and biomass burning emissions from GFED3 (van der Werf et al., 2010). We scaled the

341 original total anthropogenic NH_3 emissions from HTAP v2 using the MASAGE monthly

342 livestock/agriculture emission ratio (Figure S1, originally for the year 2005-2008 with

343 a resolution at $2.5^o \times 2.0^o$) (Paulot et al., 2014) as our prior livestock NH_3 emissions,

344 with diurnal variability calculated following Zhu, Henze, Bash, Jeong, et al. (2015). For

345 the initial guess of fertilizer application rate, we used an annual fertilizer application rate

346 for 2013 from Lu et al. (2017), which is the most up-to-date gridded data. Only a neg-

347 ligible increase ($< 3.4\%$) was found in N-fertilizer consumption over EU27 from 2013 to

348 2016 (`https://ec.europa.eu/eurostat/databrowser/view/aei_fm_usefert/default/`

349 `table?lang=en`). This annual fertilizer application rate was further scaled to daily val-

350 ues using day-to-day variation derived from MODIS EVI product (Zhu, Henze, Bash,

351 Jeong, et al., 2015). To compare with those from uni-di, NH_3 emissions (F_{emis}) and de-

352 position (F_{dep}) from bi-di were calculated using Eq.(1) and Eq.(2), respectively, follow-

353 ing Zhu, Henze, Bash, Jeong, et al. (2015) and Bash et al. (2013):

$$F_{emis} = \left. \frac{C_c}{R_a + 0.5R_{inc}} \right|_{C_a=0}, \qquad \text{Eq.(1)}$$

$$F_{dep} = \left. \frac{C_c - C_a}{R_a + 0.5R_{inc}} \right|_{C_{st}=0, C_g=0}, \qquad \text{Eq.(2)}$$

354 where C_a, C_{st}, C_g are the NH$_3$ concentrations in the air, soil and leaf stomata, respec-

355 tively. C_c is the canopy compensation point. R_a and R_{inc} are the aerodynamic resistance

356 and the in-canopy aerodynamic resistance, respectively. F_{emis} represents surface-to-air

357 flux in the bi-di scheme when the air concentration is assumed to be zero; F_{dep} is the air-

358 to-surface flux when the surface concentration is assumed to zero. $F_{emis} + F_{dep}$ is the

359 net flux from bi-di. By splitting the net flux into F_{emis} and F_{dep}, we can compare bi-

360 di emissions and deposition with those from uni-di in a comparable manner. To drive

361 uni-di simulations with the same prior emissions from bi-di, we first ran bi-di simulations

362 without optimization, saved the NH$_3$ emissions, and then used these NH$_3$ emissions as

363 the prior NH$_3$ emissions for uni-di simulations.

364   The bi-di NH$_3$ flux scheme (Zhu, Henze, Bash, Jeong, et al., 2015) is explicitly ap-

365 plied to fertilizer application. We calculated the NH$_3$ emission potential in fertilized soil

366 using soil pH and soil NH$_4^+$ concentration. We updated the soil pH from an older ver-

367 sion of the World Soil Information dataset used in Zhu, Henze, Bash, Jeong, et al. (2015)

368 to a more recent dataset (Hengl et al., 2017), which has been constrained using long-term

369 soil profile measurements (Batjes et al., 2020). In contrast, livestock NH$_3$ emissions are

370 implicitly involved in the bi-di process via their impact on simulated surface NH$_3$ con-

371 centrations and deposition to soil, with the latter serving as a NH$_4^+$ reservoir for bi-di

372 NH$_3$ flux (Zhu, Henze, Bash, Jeong, et al., 2015). Previous studies (Denmead & Freney,

373 1992; Liss & Galloway, 1993; Quinn et al., 1996; Larsen et al., 2001) have shown sim-

374 ilar bi-di NH$_3$ exchange between the atmosphere and surface water. Although the air-

375 water exchange of NH$_3$ is based on Henry's Law, it is also determined by the difference

376 between the atmospheric concentration and the "effective" concentration in the surface

377 water, whereby the NH$_3$ flux can be upward emission and downward deposition and thus

378 is similar to our bi-di scheme here. Therefore, we also apply the compensation point-based

379 bi-di scheme to water grid cells in our model following a previous study (Wichink Kruit

380 et al., 2012). In general, the resulting NH$_3$ emissions from water grid cells are negligi-

381 ble except some coastal grid cells (Figures 4 and 6) and the spatial distribution of NH$_3$

emissions from coastal grids to remote ocean grids is also consistent with those of simulated and observed NH_3 emission potential (Γ) in the water in Wichink Kruit et al. (2012). Overall, this bi-di NH_3 flux scheme generally increases the effective lifetime of atmospheric NH_3 and early afternoon concentrations (Figure 3 (i)-(l)), and thus it is expected to lead to lower top-down NH_3 emission estimates compared to those derived using uni-di NH_3 emissions.

Figure 2 shows that the application of bi-di (red solid line) in GEOS-Chem improved the simulated diurnal cycle during most of the year (especially from April to September) compared to uni-di (red dotted line) when evaluated against surface NH_3 measurements at a background site [$48^o56'$ N, $13^o25'$ E, 807 m a.s.l.] in Germany. The correlation coefficient (R) between monthly mean hourly NH_3 measurements and our prior bi-di simulation ranges from 0.59 to 0.96 from February to November, compared to our prior uni-di R ranging from -0.29 to 0.95. The improved simulated diurnal variation of NH_3 is very important for the assimilation of sun-synchronous satellite measurements as satellite data is used only once or twice per day; hence, the model's native diurnal variability has to be assumed to be correct. The prior bi-di simulation also shows a better performance in reproducing domain and nation average monthly means of surface NH_3 measurements and of NH_x wet deposition measurements for most of Europe in 2016 with reduced normalized mean error and similar correlation coefficient compared to the prior uni-di simulation (see Figures 10 and 11).

We correspondingly updated the GEOS-Chem adjoint model for the bi-di scheme. Additionally, we constructed the adjoint of run-off into waterways of deposited NH_4^+ before it entered the soil as well as the deposition-associated source and the nutrification-associated sink of NH_4^+ in the soil. We propagated these adjoint gradients back to the wet and dry deposition adjoint modules, all of which were absent from the original bi-di adjoint code (Zhu, Henze, Bash, Jeong, et al., 2015). We calculated the gradients of simulated NH_3 to fertilizer application rates and soil pH in addition to the gradients with respect to anthropogenic emissions (excluding fertilizer application), biomass burning emissions, and natural emissions. We validated our bi-di adjoint gradients with respect to fertilizer application rate and pH scale factors as well as to livestock emission scale factor for the Europe domain at $0.3125^o \times 0.25^o$ using finite difference gradients (Figure S2), which were found to be in adequate agreement ($R^2 \geq 0.99$, slope $\simeq 1.00$).

3.3 Design of inversion experiments

We applied the updated GEOS-Chem model and its adjoint to conduct a 4D-Var inversion using CrIS NH_3 profile measurements in 2016 following Cao et al. (2020). In our 4D-Var inversion, we optimized scale factors of NH_3 emissions and fertilizer application rate but not soil pH, as the latter has already been directly constrained using soil pH measurements (Hengl et al., 2017). The regularization parameter γ, which is introduced to balance the observation and penalty terms in our 4D-Var inversion, was calculated via multiplying the γ in Cao et al. (2020) by the cost function ratio at the first iteration ($\frac{J^1_{this\ study}}{J^1_{Cao\ et\ al.\ 2020}}$). We used the sum of smoothing and measurement error from the CrIS v1.5 retrieval product as the observation error covariance matrix ($\boldsymbol{S_o}$). Due to lack of quantitative knowledge of our prior emission uncertainties, the diagonal elements of our prior emission error covariance matrix ($\boldsymbol{S_a}$) are assumed to be 100% and the correlation length is assumed to be 100 km in latitudinal and longitudinal directions. For more details about the 4D-Var inversion, please refer to Cao et al. (2020).

To explore the impacts of different dry deposition schemes on posterior NH_3 emissions, we conducted two inversion experiments as shown in Table 1. IE_uni utilized uni-di, while IE_bi deployed bi-di. For both inversions, the same input parameters (including prior emissions, γ, $\boldsymbol{S_a}$ and $\boldsymbol{S_o}$) were used.

4 Results and discussion

4.1 Prior and posterior NH_3 simulations compared to CrIS observations

We start the analysis of our results by comparing the prior NH_3 simulations to CrIS observations. Figures 1 (e)-(l) show prior uni-di and bi-di simulations of monthly mean surface NH_3 concentrations averaged from 13:00-14:00 local time during March, June, September and December 2016, respectively. Both of our prior simulations using the uni-di scheme (hereafter H(Prior_uni)) and the bi-di scheme (hereafter H(Prior_bi)) generally capture CrIS-observed seasonality and spatial variability (R ranging from 0.85 to 0.90 during warm months), with higher NH_3 concentrations found during warm months (especially in September) over agricultural areas. However, Figs. 3 (a)-(h) show that our prior simulations failed to reproduce CrIS surface NH_3 concentration magnitudes, with substantial overestimation over central Europe year round and underestimation over Northern and Southern Europe during warm months. H(Prior_bi) is generally higher than H(Prior_uni)

over most of Europe throughout the year (Fig. 3 (i)-(l)) due to the increased NH_3 life-time in the bi-di simulation, with better agreement (NME ranging from 0.14 to 0.26) with CrIS NH_3 during warm months compared to H(Prior_uni) (NME ranging from 0.16 to 0.32).

The discrepancies between simulated NH_3 and CrIS observations as mentioned above were generally reduced after emission optimization. Figures 1 (m)-(t) show monthly mean surface NH_3 simulations driven by posterior NH_3 emissions derived from CrIS NH_3 pro-files from inversion experiments IE_uni and IE_bi. The posterior uni-di NH_3 simulation (H(Posterior_uni)) was simulated using the uni-di scheme and was driven by posterior NH_3 emissions derived using the uni-di scheme. Correspondingly, our posterior bi-di NH_3 simulation (H(Posterior_bi)) was simulated using the bi-di scheme and was driven by pos-terior NH_3 emissions derived using the bi-di scheme. Compared to H(Prior_uni) and H(Prior_bi), H(Posterior_uni) and H(Posterior_bi) better reproduced CrIS-observed NH_3 with slightly increased R (0.88 to 0.96 during warm months) and significantly decreased NME (rang-ing from 0.11 to 0.15) throughout the year with the exception of December. Figures 3 (m)-(t) show improvement in posterior NH_3 simulations across most of the European do-main during most of the year, especially over areas with intense agricultural practices during warm months. Significant differences remained on the eastern edge of the domain for the posterior simulations (Figure 3), which is a consequence of the boundary condi-tion from the coarse simulation ($2^o \times 2.5^o$) being held constant.

4.2 Posterior NH_3 emissions

In this section we discuss the similarity and difference between the posterior and the prior anthropogenic NH_3 emissions, and those between the posterior emissions de-rived using uni-di and bi-di schemes, in terms of spatial distribution, seasonal variation and emission magnitude.

Figures 4 (a)-(l) compare the posterior monthly anthropogenic NH_3 emissions from our inversion experiments (IE_uni and IE_bi) to the prior emissions during March, June, September and December 2016. Posterior NH_3 emissions derived using both uni-di (Pos-terior_uni) and bi-di (Posterior_bi) schemes have similar spatial distribution as the prior emissions throughout the year, with generally larger emissions (> 2 kg N ha^{-1} month^{-1}) over Germany, western France, North Italy, the Netherlands, Ireland and the UK. How-

476 ever, Fig. 4 (m)-(t) shows that heterogeneous emission adjustments occurred across the

477 European domain year round in both the Posterior_uni and Posterior_bi emissions, with

478 decreases of -10% to -50% found over central Europe and increases of 10% to 400% found

479 over most of the rest of Europe during warm months. In December, much of Europe wit-

480 nessed a decrease between -10% to -50%.

481 Also shown in Figure 4, is the difference between monthly Posterior_bi and Pos-

482 terior_uni anthropogenic NH_3 emissions over Europe for March, June, September and

483 December 2016. The Posterior_bi emissions are generally smaller than the Posterior_uni

484 emissions by a factor of 1.1 to 2.0 over most of the domain throughout the year owing

485 to increased lifetime of NH_3 in the bi-di simulations, while some exceptions (higher by

486 a factor of 1.1 to 1.3) occurred at small scales (e.g Ireland and Denmark) during March

487 and September likely because the global convergence was reached earlier than local con-

488 vergence during the course of our 4D-Var inversion, which means that the sum of the

489 error-weighted residuals across the European domain significantly reduced while some

490 local residuals may have not been completely reduced yet.

491 Europe not only incurred spatially-varying adjustments in emissions but also temporally-

492 varying adjustments. Figure 5 compares the posterior monthly anthropogenic NH_3 emis-

493 sions from inversion experiments IE_uni and IE_bi to the prior monthly estimates for EU25,

494 UK, the Netherlands, and Switzerland at regional and national scales in 2016. EU25 con-

495 sists of 25 European Union member countries (see caption of Fig. 5 for details). Both

496 the Posterior_uni and Posterior_bi emissions generally have similar seasonality as the prior

497 monthly emissions, with larger emissions found in warm months and smaller emissions

498 found in cold months, except that the posterior emissions identified an enhanced spring-

499 time peak, which is most likely related to substantial fertilizer use and manure applica-

500 tion during the crop-growing season. The general seasonal patterns of our posterior emis-

501 sions are more consistent with those of agricultural NH_3 emissions over some European

502 countries in TNO, CAMS-TEMPO and UK NAEI inventories (Denier van der Gon et

503 al., 2011; Guevara et al., 2021; Marais et al., 2021) and those constrained by satellite NH_3

504 observations (Marais et al., 2021), and are less consistent with that from Backes et al.(2016)

505 which shows a second sharp peak in September with similar magnitude as that in the

506 spring. However, their evaluation against surface NH_3 concentrations at five sites sug-

507 gests that Backes et al. (2016) tends to significantly overestimate NH_3 emissions in the

508 peaks, whereas our evaluation against domain-averaged measurements shows that our

monthly posterior NH_3 emissions generally enable the model to capture the seasonal cycle and magnitude of observed surface NH_3 and NH_x wet deposition (Fig. 10 (a) and (b) and Fig. 11 (a) and (b)). In this study the posterior emissions are generally larger than the prior emissions by a factor of 1.1 to 2.4 over EU25, the UK, and the Netherlands during most of the year, especially in spring and summer, while they are consistently lower than the prior emissions by 15% to 49% over Switzerland year round except Posterior_uni in July. The Posterior_bi emissions for EU25, UK, the Netherlands, and Switzerland are generally smaller than the Posterior_uni emissions by a factor of 1.01 to 1.52 throughout the year except those for the UK in March and October and those for the Netherlands in January, which was likely caused by the difference in global and local convergence in our emission optimization as mentioned above.

Finally, a comparison between the posterior and the prior anthropogenic emissions at an annual scale is displayed in Figure 6. The Posterior_uni and Posterior_bi anthropogenic NH_3 emissions have similar spatial patterns as the prior emissions, but are generally lower by 10% to 50% over central Europe (e.g. North Italy) and higher by a factor of 1.1 to 3.0 over most of the rest of Europe, especially over Ireland, Britain, Denmark, North Germany, and western France. The Posterior_bi annual emissions are generally smaller than the Posterior_uni emissions across most of the domain by 10% to 40% except some coastal grids due to bi-di emissions from water body near high-emission land cells. These high bi-di emissions over coastal grids are similar to those reported at the Chesapeake Bay (the largest estuary in the United States) (Larsen et al., 2001) and are also consistent with the higher simulated NH_3 concentrations with bi-di compared to those without bi-di in the coastal area of the North Sea (Wichink Kruit et al., 2012).

Overall, these emission adjustments led to smaller gaps between simulated NH_3 and CrIS observations for both uni-di and bi-di models and thus better consistency (Figure 3 (u)-(x)) between early afternoon NH_3 simulations using uni-di and bi-di. Figures 1 (e)-(t) and 3 (a)-(x) show that H(Posterior_uni) and H(Posterior_bi) had similar agreement with CrIS NH_3 observations after assimilation of CrIS NH_3 despite H(Prior_uni) and H(Prior_bi) having significantly different mismatches with CrIS NH_3 during warm months, especially during September (Fig. 3 (c) and (g)). Meanwhile, significant differences were found between the Posterior_uni and Posterior_bi monthly emissions (Fig. 4) and between the simulated hourly surface NH_3 concentrations driven by Posterior_uni and Posterior_bi emissions (Fig. 2). This contrast demonstrates the extent to which data assimilation can cor-

542 rect model simulated concentrations while also revealing how it may compensate for mech-

543 anistic biases in the model, such as the omission of NH_3 bi-di exchange. The amount by

544 which the posterior monthly emissions at regional and national scales (Figure 5) differ

545 in this case provides a means of quantifying the uncertainty in previous top-down stud-

546 ies that did not include bi-di, which we find to be [+22%, +26%] for EU25, [+4%,+22%]

547 for the UK, [+18%, +27%] for the Netherlands, [+1%, +34%] for Switzerland during warm

548 months (from April to September) when the bi-di scheme is expected to averagely have

549 larger and more frequent upward flux due to higher temperature and more fertilizer and

550 manure application across most of the Europe. Also, these differences in posterior emis-

551 sions between bi-di and uni-di can be interpreted as the differences between the effec-

552 tive lifetimes of NH_3 in uni-di and bi-di schemes since the posterior NH_3 columns con-

553 centrations from these two simulations are generally close to each other across most of

554 the domain throughout the year (Fig. 3 (u)-(x)).

4.3 Comparison with previous anthropogenic NH_3 emission estimates

556 Figure 7 compares the posterior annual total anthropogenic emission estimates from

557 the inversion experiments IE_uni and IE_bi with previous emission estimates for EU25,

558 UK, the Netherlands, and Switzerland. The Posterior_uni estimates of annual total an-

559 thropogenic emissions from EU25, the UK, and the Netherlands are 3534 Gg N a^{-1}, 332

560 Gg N a^{-1}, and 119 Gg N a^{-1}, respectively, generally larger than our prior estimates and

561 the HTAP v2 and CEIP estimates by a factor of 1.1 to 2.0, while the Posterior_uni es-

562 timate for Switzerland is significantly smaller than these bottom-up estimates by a fac-

563 tor of 1.2 to 1.8. In contrast, the Posterior_bi estimates of EU25 and the Netherlands

564 are 2850 Gg N a^{-1} and 100 Gg N a^{-1}, respectively, much closer (< 2% difference for EU25,

565 10% difference for the Netherlands) to the HTAP v2 and CEIP estimates and a recent

566 improved dynamic agricultural emission estimate (95 Gg N a^{-1} for the Netherlands) from

567 Ge et al. (2020). While the Posterior_bi emission estimate for the UK is significantly larger

568 than these bottom-up estimates by a factor of 1.3 to 1.8, the Posterior_bi emission es-

569 timate for Switzerland is consistently smaller than these bottom-up estimates by a fac-

570 tor of 1.4 to 2.1. The Posterior_bi annual total anthropogenic emissions are smaller than

571 the Posterior_uni estimates over EU25, the UK, the Netherlands, and Switzerland by 10%-

572 20%.

573   Our Posterior_uni (332 Gg N a^{-1}) and Posterior_bi (298 Gg N a^{-1}) estimates for

574 the UK are at the lower end of the recent satellite-derived anthropogenic NH$_3$ emission

575 estimate range between 315 (IASI) and 516 (CrIS v1.6) Gg N a^{-1} by Marais et al. (2021).

576 The large difference between our CrIS-derived estimates and the CrIS-based estimate

577 from Marais et al. (2021) is most likely caused by the different methods to calculate the

578 top-down emissions: we used a Bayesian inversion in which the prior information imposes

579 a penalty term on the emission optimization, whereas Marais et al. (2021) directly rescale

580 emissions using the column ratio between CrIS NH$_3$ and GC NH$_3$.

581 ### 4.4 Cross-validation using surface NH$_3$ and NH$_x$ wet deposition mea-
582 surements

583   We evaluate the posterior NH$_3$ emissions by comparing the prior and posterior sim-

584 ulations against measurements of surface NH$_3$ and NH$_x$ wet deposition in 2016 from sites

585 across Europe including the EMEP monitoring network, the LML and MAN networks

586 in the Netherlands, the NAMN network in the UK, the Switzerland national monitor-

587 ing network, the Danish Background Air Quality Monitoring Program and some short-

588 term campaign sites and long-term monitoring sites in France, the UK, and Germany.

589 We first filtered out sites with monthly mean values beyond the monthly domain aver-

590 age by three times the standard deviation in order to reduce impacts from outliers. Then

591 we averaged multiple sites within one model grid before comparing between simulations

592 and measurements. In the comparison against NH$_x$ wet deposition measurements, sim-

593 ulated NH$_x$ wet deposition consists of wet deposition of aerosol-phase NH$_4^+$ and gas-phase

594 NH$_3$. To remove the bias caused by the difference between measured and simulated pre-

595 cipitation, we scaled the measured NH$_x$ wet deposition by the ratio of modeled to mea-

596 sured precipitation, $(\frac{P_{model}}{P_{measurement}})^{0.6}$, following Paulot et al. (2014). We compared sim-

597 ulated NH$_x$ wet deposition to measurements with $\frac{P_{model}}{P_{measurement}}$ between 0.25 and 4.0

598 (Paulot et al., 2014) for EMEP sites.

599   In general, the posterior NH$_3$ emissions improve the model's ability to present ob-

600 served seasonality in surface NH$_3$ concentrations and NH$_x$ wet deposition throughout

601 the European domain. Figure 8 shows the correlation coefficient between monthly mean

602 simulations and measurements of surface NH$_3$ and NH$_x$ wet deposition for each site. The

603 first two columns of Figure 8 show that our prior uni-di simulation and prior bi-di sim-

604 ulation well reproduce the seasonal variability of NH$_x$ wet deposition measurements across

Europe, but poorly capture the seasonality of surface NH_3 observations across Europe, especially in the Netherlands, where none of the 70+ sites have a correlation coefficient (R) exceeding 0.5. The third and fourth columns of Figure 8 show that the emission optimization in our inversion experiments enables both our uni-di model and bi-di model to better reproduce the observed monthly variability of surface NH_3 for most sites across the domain, especially those located in the Netherlands and the UK. The number of sites with R for surface NH_3 measurements exceeding 0.5 increased from about 10 to approximately 30 over Europe (Figure 8) (a)-(d)), from 0 to 21-40 over the Netherlands (Figure 8) (e)-(h)), from 13-15 to 40-42 over the UK (Figure 8) (i)-(l)), and from 5 to 12-18 over Switzerland (Figure 8) (m)-(p)). In comparison, the improvement in simulating the seasonality of NH_x wet deposition (Figure 8) (q)-(t)) is moderate, with the number of sites with R exceeding 0.5 increased by less than 10 for Europe. This is likely due to the prior simulations capturing the seasonality of NH_x wet deposition well.

Figure 9 show normalized mean bias (NMB) of the annual mean of the prior and posterior monthly simulations relative to the annual mean of the monthly measurements of surface NH_3 and NH_x wet deposition, respectively, for each site across Europe. The first two columns of Figure 9 show that our prior uni-di and bi-di simulations generally have variable bias compared to the annual mean surface NH_3 measurements across most of Europe, except that a nation-wide negative bias is identified in the Netherlands. Our prior uni-di and bi-di NH_x wet deposition is generally lower than NH_x wet deposition measurements at most of the European sites. The third and fourth columns of Figure 9 show that slight to significant improvements are found in posterior uni-di and bi-di simulations of surface NH_3 and NH_x wet deposition across most of the domain, especially in the Netherlands, although Switzerland witnessed a slightly worse performance in posterior surface NH_3 likely due to the difficulty in both the model and remote sensing data presented by complex topography. The number of sites with absolute NMB exceeding 0.5 is reduced by a factor of 1.1 to 3.2 in the posterior surface NH_3 simulations over the Netherlands and the UK and in posterior NH_x wet deposition simulations across the whole Europe. The negative biases at most of the densely-distributed national monitoring sites across the Switzerland and the Netherlands in the posterior NH_3 simulations (Fig. 9 (g)-(h) and (o)-(p)) are also potentially partly owing to the fact that some of those national sites are located near animal housing or farm land (Sutton et al., 2015) and our model resolution of about 25 km^2 is unable to capture the local sharp gradients of NH_3 con-

638 centrations. On the other hand, the high bias across most of the UK sites and EMEP

639 sites in the posterior NH_3 simulations (Fig. 9 (k)-(l) and (c)-(d)) is likely caused by the

640 fact that the CrIS v1.5 retrieval used in this study did not include non-detect pixels and

641 is thus biased high over background areas and cloudy areas (good-weather bias), such

642 as the UK. An updated CrIS v1.6 retrieval including the non-detects has been used to

643 constrain the UK emissions in a recent study (Marais et al., 2021) and was found to re-

644 duce the high bias to some extent. While we do recommend using CrIS v1.6 for future

645 studies, we were not able to use the v1.6 product for this study as it was not publicly

646 available at the time our calculations were conducted. The inclusion of non-detects will

647 unlikely significantly impact the uncertainty associated with the NH_3 flux scheme in our

648 top-down emissions as we use the same satellite data for both uni-di and bi-di inversions.

649 Further comparison between the prior and posterior simulations of surface NH_3 and

650 monthly mean measurements at regional and national scales is shown in Figure 10. Fig. 10

651 (a) and (b) show that monthly mean domain average of surface NH_3 measurements over

652 the EU are generally larger in warm months and lower in cold months, which is consis-

653 tent with CrIS surface NH_3 observations (Fig. 1 (a)-(d)) and suggests larger NH_3 emis-

654 sions in warm months and smaller emissions in cold months in a general sense. More-

655 over, the unusual September/June contrast in surface NH_3 observations (Fig. 10 (a) and

656 (b)) is also consistent with that in CrIS surface NH_3 observations (Fig. 1 (b) and (c)),

657 which, however, cannot be explained by the September/June contrast in posterior emis-

658 sions (Fig. 5) but is most likely caused by the significantly larger NH_x wet deposition

659 in June than in September (Fig. 11 (a) and (b)) in 2016. Both our prior uni-di and bi-

660 di models show poor to fair skill in reproducing the monthly variation of surface NH_3

661 measurements at regional and national scales, with R between 0.42 to 0.48 for EU and

662 Switzerland and R below zero over the Netherlands and the UK. Prior uni-di and bi-di

663 monthly simulations are significantly lower than monthly mean regional and national av-

664 erages throughout most of the year except cold months, resulting in annual regional and

665 national NMB values ranging from -0.13 to -0.52 in uni-di simulations and from 0.01 to

666 -0.43 in bi-di simulations. Generally, the emission optimization enabled better uni-di and

667 bi-di simulations of surface NH_3 with a substantially increased correlation coefficient be-

668 tween monthly simulations and monthly mean spatial averages of surface NH_3 measure-

669 ments and significantly reduced normalized mean error over most of the European coun-

670 tries except Switzerland, which experienced a slight increase in the annual NME.

671   Improvements in the posterior simulations are found in comparison with spatially

672 averaged monthly mean NH_x wet deposition measurements over Europe as shown in Fig-

673 ure 11, similar to ambient NH_3 results. Domain average monthly mean NH_x wet depo-

674 sition measurements over Europe is higher in warm months and shows a larger peak in

675 the spring and a smaller peak in late autumn, likely due to the combined impacts of the

676 seasonality of agricultural emissions and precipitation. Both our prior uni-di and bi-di

677 monthly simulations can capture the observed seasonal variation of NH_x wet deposition

678 measurements at regional and national scales with R ranging between 0.87 and 0.90 but

679 are significantly lower than the measurements during most of the year (especially in warm

680 months) with annual NMB ranging between -0.40 and -0.50. Our posterior NH_3 emis-

681 sions improve the overall ability of the model to reproduce NH_x wet deposition measure-

682 ments at regional and national scales with significantly reduced NMB (-0.27 to -0.29)

683 and similar high R (0.90 to 0.91) as that of prior simulations, although our posterior sim-

684 ulations still show low bias compared to the NH_x wet deposition measurements.

685   Finally, another evaluation using hourly measurements of surface NH_3 at a back-

686 ground site (Bavarian Forest National Park) in Germany (Wintjen et al., 2020) is dis-

687 played in Figure 2. As mentioned in section 4.1, the prior bi-di model better reproduces

688 the observed diurnal variability of surface NH_3 throughout most of the year, especially

689 during warm months, compared to the prior uni-di model. Both the prior uni-di and bi-

690 di models overestimate the monthly mean hourly surface NH_3 measurements year round

691 by a factor of 1.02 to 10.99. While generally having a similar diurnal cycle as the prior

692 simulations, the posterior bi-di simulation better reproduces the magnitude of monthly-

693 averaged hourly surface NH_3 measurements in most of the year, reducing the monthly

694 NMB to between 0.28 to 4.36. In contrast, the Posterior_uni emissions generally degrade

695 the uni-di model's performance in reproducing the magnitude of surface NH_3 observa-

696 tions at a monthly scale, increasing the monthly NMB by a factor of 1.3 to 29.5 during

697 most of the year except September, November and December. Although our optimiza-

698 tions reduced the monthly NMB in December by more than a factor of 2 for both inver-

699 sions, large NMB values were still found in the posterior simulations, which is likely ow-

700 ing to 1) the poor temporal coverage of in-situ measurements during December and 2)

701 the high bias in CrIS v1.5 over background (low-concentration) areas (especially in win-

702 ter months) due to exclusion of non-detects as mentioned above.

5 Conclusions

This study presents the first 4D-Var inversion of NH_3 sources using a bi-di NH_3 flux scheme and CrIS NH_3 measurements. The posterior annual anthropogenic NH_3 emissions have a similar spatial distribution as the prior emissions, but are generally smaller over central Europe and larger over most of the rest of Europe compared to the prior emissions. The posterior monthly emissions generally have a more pronounced springtime peak than the prior. The Posterior_bi regional and national total anthropogenic NH_3 emissions are generally less than the Posterior_uni emissions by 10% to 20% for EU25, the UK, the Netherlands, and Switzerland at an annual scale, while up to -34% difference is found at a monthly scale. These differences can provide a rough estimate of the uncertainty associated with NH_3 flux estimates in previous inverse modeling studies using uni-di only.

The Posterior_bi annual regional total anthropogenic NH_3 emissions are generally within the bottom-up estimate ranges over EU25 (2275 to 2895 Gg N a^{-1}) and the Netherlands (90 to 110 Gg N a^{-1}), while the Posterior_uni estimates are greater than the upper range by 8% over the Netherlands and by 22% over the EU25. Our posterior estimates of national total anthropogenic NH_3 emissions are greater than the upper range of bottom-up estimates (169 to 237 Gg N a^{-1}) by 26% to 40% in the UK. On the other hand, our posterior estimates of national total anthropogenic NH_3 emissions are less than the lower end of bottom-up estimates (42 to 62 Gg N a^{-1}) by 17% to 31% in Switzerland, which likely has large uncertainty due to the difficulty in both the model and remote sensing data presented by the complex topography there.

Cross-validation by measurements of surface NH_3 and NH_x wet deposition from extensive sites across Europe show that our posterior emissions from inversions enable our uni-di model and bi-di model to better reproduce monthly mean measurements of NH_3 and NH_x wet deposition increasing the R between simulated and observed monthly mean regional and national averages from between -0.15 and 0.90 to between 0.47 and 0.91 and reducing the NME by a factor of 1.2 to 2.9 (except Switzerland).

While evaluation against monthly mean surface measurements of NH_3 and NH_x wet deposition show similar improvements in both bi-di and uni-di simulations after data assimilation, another evaluation (Figure 2) against hourly measurements of surface NH_3 at a background site in Germany suggests bi-di better reproduces the observed diurnal

735 variability of surface NH$_3$. The coexistence of this difference in hourly simulations of sur-

736 face NH$_3$ (Figure 2) using bi-di and uni-di and the difference between Posterior_bi and

737 Posterior_uni monthly emissions (Figures 4 and 5) and the consistency in early afternoon

738 NH$_3$ simulations using these two schemes (Figures 3 (u)-(x)) demonstrate the importance

739 of accurately simulating diurnal cycle of NH$_3$ in the assimilation of the Sun-synchronous

740 satellite observations, and calls for highly temporally resolved constraints from geosta-

741 tionary satellites.

742 While the bi-di scheme seems to better capture the diurnal variability at the back-

743 ground site in Germany, such improvements may not be ubiquitous. For comparison, dif-

744 ferent diurnal cycles were identified at urban and suburban sites at Beijing in Lan et al. (2021),

745 where generally higher concentrations of ammonia during the daytime and low concen-

746 trations during the nighttime were observed at a suburban site during most of the year

747 except autumn, while the opposite condition was found at an urban site during non-spring

748 seasons. As discussed therein, the complexity and variability of NH$_3$ diurnal cycles is ow-

749 ing to multiple competing factors including sources, chemical sinks, vertical mixing, hor-

750 izontal transport, temperature, relative humidity and other meteorological impacts; im-

751 provements made owing to bidi alone may not lead to improved simulated diurnal vari-

752 ability in all conditions.

753 It may be hard to disentangle this multitude of effects due to the sparsity of hourly

754 in-situ measurements of NH$_3$. In addition, some urban sources (e.g., vehicular emissions)

755 lead to more variable diurnal cycles in NH$_3$ concentrations (Whitehead et al., 2007) and

756 the underestimate of such vehicular sources in current bottom-up inventories (Sun et al.,

757 2017) could introduce additional uncertainty in simulating NH$_3$ diurnal cycles in urban

758 area. Overall, estimating and constraining NH$_3$ emissions would greatly benefit from ad-

759 ditional widespread hourly measurements that could be provided by geostationary satel-

760 lite observations (Clarisse et al., 2021).

761 Given the critical role of NH$_3$ in PM$_{2.5}$ formation and excessive deposition of Nr

762 and the severe nitrogen crisis some European countries are facing (Stokstad, 2019) as

763 well as the current and projected decrease of SO$_x$ and NO$_x$ emission trends and increas-

764 ing NH$_3$ emission trend in Europe, measures to be taken to reduce NH$_3$ emissions in Eu-

765 rope such as the amended National Emission Ceiling Directive (NEC) Directive (EC, 2016)

766 targeting reducing NH$_3$ emissions between 2020 and 2030 are increasingly valuable. In

the meantime, spatially and temporally resolved monitoring of NH_3 emissions at a large scale is needed for assessing the effectiveness of NH_3 abatement policies across Europe. Our 4D-Var inversion system implemented with bi-di and uni-di NH_3 flux schemes and coupled with CrIS NH_3 observations can provide comprehensive and up-to-date spatially resolved evaluation of NH_3 emissions. Moreover, up-to-date posterior NH_3 emissions can improve air quality forecasts and thus have the potential to help guide strategies for reducing $PM_{2.5}$ exposure. Operational near-real-time observations of NH_3 using satellite instruments could also be used to explore regional and global NH_3 emission trends (Shephard & Cady-Pereira, 2015; Shephard et al., 2020; Glumb et al., 2018), which may support broader adoption of environmental policy regarding Nr.

References

Amos, H. M., Jacob, D. J., Holmes, C. D., Fisher, J. A., Wang, Q., Yantosca, R. M., ... Sunderland, E. M. (2012). Gas-particle partitioning of atmospheric Hg(II) and its effect on global mercury deposition. *Atmos. Chem. Phys.*, *12*(1), 591–603. doi: 10.5194/acp-12-591-2012

Backes, A., Aulinger, A., Bieser, J., Matthias, V., & Quante, M. (2016). Ammonia emissions in europe, part i: Development of a dynamical ammonia emission inventory. *Atmospheric Environment*, *131*, 55-66. doi: https://doi.org/10.1016/j.atmosenv.2016.01.041

Bash, J. O., Cooter, E. J., Dennis, R. L., Walker, J. T., & Pleim, J. E. (2013). Evaluation of a regional air-quality model with bidirectional nh$_3$ exchange coupled to an agroecosystem model. *Biogeosciences*, *10*(3), 1635–1645. doi: 10.5194/bg-10-1635-2013

Batjes, N. H., Ribeiro, E., & van Oostrum, A. (2020). Standardised soil profile data to support global mapping and modelling (WoSIS snapshot 2019). *Earth System Science Data*, *12*(1), 299–320. Retrieved from https://essd.copernicus.org/articles/12/299/2020/ doi: 10.5194/essd-12-299-2020

Beer, R., Shephard, M. W., Kulawik, S. S., Clough, S. A., Eldering, A., Bowman, K. W., ... Worden, J. R. (2008). First satellite observations of lower tropospheric ammonia and methanol. *Geophysical Research Letters*, *35*(9). doi: https://doi.org/10.1029/2008GL033642

Behera, S. N., Sharma, M., Aneja, V. P., & Balasubramanian, R. (2013, Nov 01). Ammonia in the atmosphere: a review on emission sources, atmospheric chemistry and deposition on terrestrial bodies. *Environ. Sci. Pollut. Res.*, *20*(11), 8092–8131. doi: 10.1007/s11356-013-2051-9

Berner, A. H., & Felix, J. D. (2020). Investigating ammonia emissions in a coastal urban airshed using stable isotope techniques. *Science of The Total Environment*, *707*, 134952. doi: https://doi.org/10.1016/j.scitotenv.2019.134952

Binkowski, F. S., & Roselle, S. J. (2003). Models-3 Community Multiscale Air Quality (CMAQ) model aerosol component 1. Model description. *J. Geophys. Res.*, *108*(D6). doi: 10.1029/2001JD001409

Cao, H., Henze, D. K., Shephard, M. W., Dammers, E., Cady-Pereira, K., Alvarado, M., ... Edgerton, E. S. (2020). Inverse modeling of nh3 sources

using cris remote sensing measurements. *Environmental Research Letters*. doi: 10.1088/1748-9326/abb5cc

Chang, Y., Zou, Z., Deng, C., Huang, K., Collett, J. L., Lin, J., & Zhuang, G. (2016). The importance of vehicle emissions as a source of atmospheric ammonia in the megacity of shanghai. *Atmospheric Chemistry and Physics*, *16*(5), 3577–3594. doi: 10.5194/acp-16-3577-2016

Chen, Y., Shen, H., Kaiser, J., Hu, Y., Capps, S. L., Zhao, S., ... others (2021). High-resolution hybrid inversion of iasi ammonia columns to constrain us ammonia emissions using the cmaq adjoint model. *Atmospheric Chemistry and Physics*, *21*(3), 2067–2082. doi: 10.5194/acp-21-2067-2021

Cheng, F., Van Meter, K., Byrnes, D., & Basu, N. (2020). Maximizing us nitrate removal through wetland protection and restoration. *Nature*, 1–6. doi: 10.1038/s41586-020-03042-5

Clarisse, L., Clerbaux, C., Dentener, F., Hurtmans, D., & Coheur, P.-F. (2009). Global ammonia distribution derived from infrared satellite observations. *Nature Geoscience*, *2*(7), 479–483. doi: doi.org/10.1038/ngeo551

Clarisse, L., Van Damme, M., Clerbaux, C., & Coheur, P.-F. (2019). Tracking down global NH$_3$ point sources with wind-adjusted superresolution. *Atmos. Meas. Tech.*, *12*(10), 5457–5473. doi: 10.5194/amt-12-5457-2019

Clarisse, L., Van Damme, M., Gardner, W., Coheur, P., Clerbaux, C., Whitburn, S., ... Hurtmans, D. (2019). Atmospheric ammonia (nh3) emanations from lake natron's saline mudflats. *Sci Rep*, *9*. doi: 10.1038/s41598-019-39935-3

Clarisse, L., Van Damme, M., Hurtmans, D., Franco, B., Clerbaux, C., & Coheur, P.-F. (2021). The diel cycle of NH3 observed from the FY-4A Geostationary Interferometric Infrared Sounder (GIIRS). *Geophysical Research Letters*, *48*, e2021GL093010. doi: https://doi.org/10.1029/2021GL093010

Crippa, M., Solazzo, E., Huang, G., Guizzardi, D., Koffi, E., Muntean, M., ... Janssens-Maenhout, G. (2020). High resolution temporal profiles in the emissions database for global atmospheric research. *Scientific data*, *7*(1), 1–17. doi: 10.6084/m9.figshare.12052887

Dammers, E., McLinden, C. A., Griffin, D., Shephard, M. W., Van Der Graaf, S., Lutsch, E., ... Erisman, J. W. (2019). NH$_3$ emissions from large point sources derived from CrIS and IASI satellite observations. *Atmos. Chem. Phys.*,

865   *19*(19), 12261–12293. doi: 10.5194/acp-19-12261-2019

866 Dammers, E., Shephard, M. W., Palm, M., Cady-Pereira, K., Capps, S., Lutsch,

867   E., ... Erisman, J. W. (2017). Validation of the CrIS fast physical NH$_3$ re-

868   trieval with ground-based FTIR. *Atmos. Meas. Tech.*, *10*(7), 2645–2667. doi:

869   10.5194/amt-10-2645-2017

870 Denier van der Gon, H., Hendriks, C., Kuenen, J., Segers, A., & Visschedijk, A.

871   (2011). Description of current temporal emission patterns and sensitivity of

872   predicted aq for temporal emission patterns. *EU FP7 MACC deliverable report*

873   *D_D-EMIS_1*, *3*, 2019–07.

874 Denmead, O. T., & Freney, J. R. (1992). Transfer coefficients for water-air exchange

875   of ammonia, carbon dioxide and methane. *Ecological Bulletins*, 31–41. Re-

876   trieved from https://www.jstor.org/stable/20113103

877 Du, E., de Vries, W., Galloway, J. N., Hu, X., & Fang, J. (2014). Changes in wet

878   nitrogen deposition in the United States between 1985 and 2012. *Environ. Res.*

879   *Lett.*, *9*(9), 095004. doi: 10.1088/1748-9326/9/9/095004

880 EC. (2016). Directive 2016/2284 of the European Parliament and of the Council

881   of 14 December 2016 on the reduction of national emissions of certain atmo-

882   spheric pollutants, amending Directive 2003/35/EC and repealing Directive

883   2001/81/EC.

884 EEA. (2017). European Union emission inventory report 1990-2015 under the UN-

885   ECE Convention on Long-range Transboundary Air Pollution (LRTAP).

886 EEA. (2020). European Union emission inventory report 1990-2018 under the UN-

887   ECE Convention on Long-range Transboundary Air Pollution (LRTAP).

888 Elguindi, N., Granier, C., Stavrakou, T., Darras, S., Bauwens, M., Cao, H., ...

889   Zheng, B. (2020). Intercomparison of Magnitudes and Trends in Anthro-

890   pogenic Surface Emissions From Bottom-Up Inventories, Top-Down Esti-

891   mates, and Emission Scenarios. *Earth's Future*, *8*(8), e2020EF001520. doi:

892   https://doi.org/10.1029/2020EF001520

893 Ellermann, T., Nygaard, J., Christensen, J. H., Løfstrøm, P., Geels, C., Nielsen,

894   I. E., ... Hertel, O. (2018). Nitrogen deposition on danish nature. *Atmo-*

895   *sphere*, *9*(11). doi: 10.3390/atmos9110447

896 Ellis, R. A., Jacob, D. J., Sulprizio, M. P., Zhang, L., Holmes, C. D., Schichtel,

897   B. A., ... Lynch, J. A. (2013). Present and future nitrogen deposition to

national parks in the United States: Critical load exceedances. *Atmos. Chem. Phys.*, *13*(17), 9083–9095. doi: 10.5194/acp-13-9083-2013

Erisman, J., & Schaap, M. (2004). The need for ammonia abatement with respect to secondary pm reductions in europe. *Environmental Pollution*, *129*(1), 159-163. doi: https://doi.org/10.1016/j.envpol.2003.08.042

Erisman, J. W., Galloway, J. N., Seitzinger, S., Bleeker, A., Dise, N. B., Petrescu, A. M. R., ... de Vries, W. (2013). Consequences of human modification of the global nitrogen cycle. *Philos Trans R Soc Lond B Biol Sci*, *368*(20130116), 1–9. doi: 10.1098/rstb.2013.0116

Evangeliou, N., Balkanski, Y., Eckhardt, S., Cozic, A., Van Damme, M., Coheur, P.-F., ... Hauglustaine, D. (2021). 10-year satellite-constrained fluxes of ammonia improve performance of chemistry transport models. *Atmospheric Chemistry and Physics*, *21*(6), 4431–4451. doi: 10.5194/acp-21-4431-2021

Fenn, M. E., Bytnerowicz, A., Schilling, S. L., Vallano, D. M., Zavaleta, E. S., Weiss, S. B., ... Hanks, K. (2018). On-road emissions of ammonia: An underappreciated source of atmospheric nitrogen deposition. *Science of The Total Environment*, *625*, 909 - 919. doi: https://doi.org/10.1016/j.scitotenv.2017.12.313

Flechard, C. R., Nemitz, E., Smith, R. I., Fowler, D., Vermeulen, A. T., Bleeker, A., ... Sutton, M. A. (2011). Dry deposition of reactive nitrogen to european ecosystems: a comparison of inferential models across the nitroeurope network. *Atmospheric Chemistry and Physics*, *11*(6), 2703–2728. doi: 10.5194/acp-11-2703-2011

Galloway, J. N., Aber, J. D., Erisman, J. W., Seitzinger, S. P., Howarth, R. W., Cowling, E. B., & Cosby, B. J. (2003, 04). The Nitrogen Cascade. *BioScience*, *53*(4), 341-356. doi: 10.1641/0006-3568(2003)053[0341:TNC]2.0.CO;2

Ge, X., Schaap, M., Kranenburg, R., Segers, A., Reinds, G. J., Kros, H., & de Vries, W. (2020). Modeling atmospheric ammonia using agricultural emissions with improved spatial variability and temporal dynamics. *Atmospheric Chemistry and Physics*, *20*(24), 16055–16087. doi: 10.5194/acp-20-16055-2020

Geels, C., Andersen, H. V., Ambelas Skjøth, C., Christensen, J. H., Ellermann, T., Løfstrøm, P., ... Hertel, O. (2012). Improved modelling of atmospheric ammonia over denmark using the coupled modelling system damos. *Biogeosciences*, *9*(7), 2625–2647. doi: 10.5194/bg-9-2625-2012

Giannakis, E., Kushta, J., Bruggeman, A., & Lelieveld, J. (2019). Costs and benefits of agricultural ammonia emission abatement options for compliance with European air quality regulations. *Environ Sci Eur*, *31*(1), 93. doi: 10.1186/s12302-019-0275-0

Giannakis, E., Kushta, J., Giannadaki, D., Georgiou, G. K., Bruggeman, A., & Lelieveld, J. (2019). Exploring the economy-wide effects of agriculture on air quality and health: evidence from europe. *Science of The Total Environment*, *663*, 889–900. doi: 10.1016/j.scitotenv.2019.01.410

Gilliland, A. B., Dennis, R. L., Roselle, S. J., & Pierce, T. E. (2003). Seasonal NH$_3$ emission estimates for the eastern United States based on ammonium wet concentrations and an inverse modeling method. *J. Geophys. Res.*, *108*(D15). doi: 10.1029/2002JD003063

Glumb, R., Suwinski, L., Wells, S., Glumb, A., Malloy, R., & Colton, M. (2018). The JPSS CrIS Instrument and the Evolution of Space-Based Infrared Sounders.

Goodkind, A. L., Tessum, C. W., Coggins, J. S., Hill, J. D., & Marshall, J. D. (2019). Fine-scale damage estimates of particulate matter air pollution reveal opportunities for location-specific mitigation of emissions. *Proceedings of the National Academy of Sciences*, *116*(18), 8775–8780. doi: 10.1073/pnas.1816102116

Guevara, M., Jorba, O., Tena, C., Denier van der Gon, H., Kuenen, J., Elguindi, N., ... Pérez García-Pando, C. (2021). Copernicus atmosphere monitoring service temporal profiles (cams-tempo): global and european emission temporal profile maps for atmospheric chemistry modelling. *Earth System Science Data*, *13*(2), 367–404. doi: 10.5194/essd-13-367-2021

Heald, C. L., Collett Jr., J. L., Lee, T., Benedict, K. B., Schwandner, F. M., Li, Y., ... Pye, H. O. T. (2012). Atmospheric ammonia and particulate inorganic nitrogen over the United States. *Atmos. Chem. Phys.*, *12*(21), 10295–10312. doi: 10.5194/acp-12-10295-2012

Hengl, T., Mendes de Jesus, J., Heuvelink, G. B., Ruiperez Gonzalez, M., Kilibarda, M., Blagotić, A., ... others (2017). Soilgrids250m: Global gridded soil information based on machine learning. *PLoS one*, *12*(2), e0169748. doi: 10.1371/journal.pone.0169748

Henze, D. K., Seinfeld, J. H., & Shindell, D. T. (2009). Inverse modeling and

mapping US air quality influences of inorganic PM$_{2.5}$ precursor emissions using the adjoint of GEOS-Chem. *Atmos. Chem. Phys.*, *9*, 5877–5903. doi: 10.5194/acp-9-5877-2009

Hoesly, R. M., Smith, S. J., Feng, L., Klimont, Z., Janssens-Maenhout, G., Pitkanen, T., ... Zhang, Q. (2018). Historical (1750–2014) anthropogenic emissions of reactive gases and aerosols from the Community Emissions Data System (CEDS). *Geosci. Model Dev.*, *11*(1), 369–408. doi: 10.5194/gmd-11-369-2018

Huang, X., Song, Y., Li, M., Li, J., Huo, Q., Cai, X., ... Zhang, H. (2012). A high-resolution ammonia emission inventory in china. *Global Biogeochemical Cycles*, *26*(1). doi: https://doi.org/10.1029/2011GB004161

Hudman, R. C., Moore, N. E., Mebust, A. K., Martin, R. V., Russell, A. R., Valin, L. C., & Cohen, R. C. (2012). Steps towards a mechanistic model of global soil nitric oxide emissions: implementation and space based-constraints. *Atmospheric Chemistry and Physics*, *12*(16), 7779–7795. doi: 10.5194/acp-12-7779-2012

Janssens-Maenhout, G., Crippa, M., Guizzardi, D., Dentener, F., Muntean, M., Pouliot, G., ... Li, M. (2015). HTAP_v2.2: a mosaic of regional and global emission grid maps for 2008 and 2010 to study hemispheric transport of air pollution. *Atmos. Chem. Phys.*, *15*(19), 11411–11432. doi: 10.5194/acp-15-11411-2015

Kong, L., Tang, X., Zhu, J., Wang, Z., Pan, Y., Wu, H., ... Carmichael, G. (2019). Improved inversion of monthly ammonia emissions in china based on the chinese ammonia monitoring network and ensemble kalman filter. *Environmental Science & Technology*, *53*(21), 12529-12538. doi: 10.1021/acs.est.9b02701

Krupa, S. (2003). Effects of atmospheric ammonia (NH$_3$) on terrestrial vegetation: a review. *Environ. Pollut.*, *124*(2), 179 - 221. doi: https://doi.org/10.1016/S0269 -7491(02)00434-7

Lan, Z., Lin, W., Pu, W., & Ma, Z. (2021). Measurement report: Exploring nh$_3$ behavior in urban and suburban beijing: comparison and implications. *Atmospheric Chemistry and Physics*, *21*(6), 4561–4573. doi: 10.5194/acp-21-4561 -2021

Larsen, R. K., Steinbacher, J. C., & Baker, J. E. (2001). Ammonia exchange between the atmosphere and the surface waters at two locations in the chesa-

peake bay. *Environmental Science & Technology*, *35*(24), 4731-4738. doi: 10.1021/es010755l

Lelieveld, J., Evans, J. S., Fnais, M., Giannadaki, D., & Pozzer, A. (2015). The contribution of outdoor air pollution sources to premature mortality on a global scale. *Nature*, *525*(7569), 367–371. doi: 10.1038/nature15371

Li, Y., Schichtel, B. A., Walker, J. T., Schwede, D. B., Chen, X., Lehmann, C. M., ... Collett, J. L. (2016). Increasing importance of deposition of reduced nitrogen in the United States. *Proc. Natl. Acad. Sci. U.S.A.*, *113*(21), 5874–5879. doi: 10.1073/pnas.1525736113

Liss, P. S., & Galloway, J. N. (1993). Air-sea exchange of sulphur and nitrogen and their interaction in the marine atmosphere. In *Interactions of c, n, p and s biogeochemical cycles and global change* (pp. 259–281). Springer.

Liu, H., Jacob, D. J., Bey, I., & Yantosca, R. M. (2001). Constraints from 210Pb and 7Be on wet deposition and transport in a global three-dimensional chemical tracer model driven by assimilated meteorological fields. *J. Geophys. Res.*, *106*(D11), 12109-12128. doi: 10.1029/2000JD900839

Liu, M., Huang, X., Song, Y., Xu, T., Wang, S., Wu, Z., ... Zhu, T. (2018). Rapid SO_2 emission reductions significantly increase tropospheric ammonia concentrations over the North China Plain. *Atmos. Chem. Phys.*, *18*(24), 17933–17943. doi: 10.5194/acp-18-17933-2018

Lolkema, D., Noordijk, H., Stolk, A., Hoogerbrugge, R., van Zanten, M., & van Pul, W. (2015). The measuring ammonia in nature (man) network in the netherlands. *Biogeosciences*, *12*(16), 5133–5142. doi: 10.5194/bg-12-5133-2015

Lonati, G., & Cernuschi, S. (2020). Temporal and spatial variability of atmospheric ammonia in the lombardy region (northern italy). *Atmospheric Pollution Research*, *11*(12), 2154 - 2163. (World Clean Air Congress 2019) doi: 10.1016/j.apr.2020.06.004

Lu, C., & Tian, H. (2017). Global nitrogen and phosphorus fertilizer use for agriculture production in the past half century: shifted hot spots and nutrient imbalance. *Earth System Science Data*, *9*(1), 181–192. doi: 10.5194/essd-9-181-2017

Mao, J., Jacob, D. J., Evans, M. J., Olson, J. R., Ren, X., Brune, W. H., ... Carouge, C. (2010). Chemistry of hydrogen oxide radicals (ho_x) in the Arc-

tic troposphere in spring. *Atmos. Chem. Phys.*, *10*(13), 5823–5838. doi: 10.5194/acp-10-5823-2010

Marais, E. A., Pandey, A. K., Damme, M. V., Clarisse, L., Coheur, P.-F., Shephard, M. W., ... Yu, F. (2021). UK ammonia emissions estimated with satellite observations and GEOS-chem. *Under review, Journal of Geophysical Research: Atmospheres*. doi: 10.1002/essoar.10507043.1

McDuffie, E. E., Smith, S. J., O'Rourke, P., Tibrewal, K., Venkataraman, C., Marais, E. A., ... Martin, R. V. (2020). A global anthropogenic emission inventory of atmospheric pollutants from sector- and fuel-specific sources (1970–2017): an application of the Community Emissions Data System (CEDS). *Earth System Science Data*, *12*(4), 3413–3442. doi: 10.5194/essd-12-3413-2020

Miyazaki, K., Bowman, K., Sekiya, T., Eskes, H., Boersma, F., Worden, H., ... Ogochi, K. (2019). Chemical reanalysis products. *Jet Propulsion Laboratory*. doi: 10.25966/9qgv-fe81

Miyazaki, K., Bowman, K., Sekiya, T., Eskes, H., Boersma, F., Worden, H., ... Ogochi, K. (2020). Updated tropospheric chemistry reanalysis and emission estimates, TCR-2, for 2005–2018. *Earth System Science Data*, *12*(3), 2223–2259. doi: 10.5194/essd-12-2223-2020

Myhre, G., Berglen, T. F., Johnsrud, M., Hoyle, C. R., Berntsen, T. K., Christopher, S. A., ... Yttri, K. E. (2009). Modelled radiative forcing of the direct aerosol effect with multi-observation evaluation. *Atmos. Chem. Phys.*, *9*(4), 1365–1392. doi: 10.5194/acp-9-1365-2009

Nah, T., Guo, H., Sullivan, A. P., Chen, Y., Tanner, D. J., Nenes, A., ... Weber, R. J. (2018). Characterization of aerosol composition, aerosol acidity, and organic acid partitioning at an agriculturally intensive rural southeastern US site. *Atmos. Chem. Phys.*, *18*(15), 11471–11491. doi: 10.5194/acp-18-11471-2018

Nair, A. A., & Yu, F. (2020). Quantification of atmospheric ammonia concentrations: A review of its measurement and modeling. *Atmosphere*, *11*(10). doi: 10.3390/atmos11101092

Neirynck, J., & Ceulemans, R. (2008). Bidirectional ammonia exchange above a mixed coniferous forest. *Environmental Pollution*, *154*(3), 424 - 438. (Reduced

Nitrogen in Ecology and the Environment) doi: https://doi.org/10.1016/j.envpol.2007.11.030

Nemitz, E., Milford, C., & Sutton, M. A. (2001). A two-layer canopy compensation point model for describing bi-directional biosphere-atmosphere exchange of ammonia. *Quarterly Journal of the Royal Meteorological Society*, *127*(573), 815-833. doi: https://doi.org/10.1002/qj.49712757306

Park, R. J., Jacob, D. J., Field, B. D., Yantosca, R. M., & Chin, M. (2004). Natural and transboundary pollution influences on sulfate-nitrate-ammonium aerosols in the United States: Implications for policy. *J. Geophys. Res.*, *109*(D15). doi: 10.1029/2003JD004473

Paulot, F., Jacob, D. J., Pinder, R. W., Bash, J. O., Travis, K., & Henze, D. K. (2014). Ammonia emissions in the United States, European Union, and China derived by high-resolution inversion of ammonium wet deposition data: Interpretation with a new agricultural emissions inventory (MASAGE_NH3). *J. Geophys. Res.*, *119*(7), 4343-4364. doi: 10.1002/2013JD021130

Pinder, R. W., Adams, P. J., Pandis, S. N., & Gilliland, A. B. (2006). Temporally resolved ammonia emission inventories: Current estimates, evaluation tools, and measurement needs. *J. Geophys. Res.*, *111*(D16). doi: 10.1029/2005JD006603

Pleim, J. E., Bash, J. O., Walker, J. T., & Cooter, E. J. (2013). Development and evaluation of an ammonia bidirectional flux parameterization for air quality models. *Journal of Geophysical Research: Atmospheres*, *118*(9), 3794-3806. doi: https://doi.org/10.1002/jgrd.50262

Pleim, J. E., Ran, L., Appel, W., Shephard, M. W., & Cady-Pereira, K. (2019). New bidirectional ammonia flux model in an air quality model coupled with an agricultural model. *Journal of Advances in Modeling Earth Systems*, *11*(9), 2934-2957. doi: https://doi.org/10.1029/2019MS001728

Quinn, P., Barrett, K., Dentener, F., Lipschultz, F., & Six, K. (1996). Estimation of the air/sea exchange of ammonia for the north atlantic basin. In *Nitrogen cycling in the north atlantic ocean and its watersheds* (pp. 275–304). Springer. Retrieved from https://www.jstor.org/stable/1469232

Schiferl, L. D., Heald, C. L., Van Damme, M., Clarisse, L., Clerbaux, C., Coheur, P.-F., ... Eilerman, S. J. (2016). Interannual variability of ammonia con-

centrations over the United States: Sources and implications. *Atmos. Chem. Phys.*, *16*(18), 12305–12328. doi: 10.5194/acp-16-12305-2016

Seitler, E., & Meier, M. (2021). Ammoniak-Immissionsmessungen in der Schweiz 2000 bis 2020. Retrieved from `https://www.bafu.admin.ch/bafu/en/home/topics/air/publications-studies/studies.html`

Shephard, M. W., & Cady-Pereira, K. E. (2015). Cross-track Infrared Sounder (CrIS) satellite observations of tropospheric ammonia. *Atmos. Meas. Tech.*, *8*(3), 1323–1336. doi: 10.5194/amt-8-1323-2015

Shephard, M. W., Cady-Pereira, K. E., Luo, M., Henze, D. K., Pinder, R. W., Walker, J. T., ... Clarisse, L. (2011). TES ammonia retrieval strategy and global observations of the spatial and seasonal variability of ammonia. *Atmos. Chem. Phys.*, *11*(20), 10743–10763. doi: 10.5194/acp-11-10743-2011

Shephard, M. W., Dammers, E., Cady-Pereira, K. E., Kharol, S. K., Thompson, J., Gainariu-Matz, Y., ... Zheng, Q. (2020). Ammonia measurements from space with the cross-track infrared sounder: characteristics and applications. *Atmospheric Chemistry and Physics*, *20*(4), 2277–2302. Retrieved from `https://acp.copernicus.org/articles/20/2277/2020/` doi: 10.5194/acp-20-2277-2020

Skjøth, C. A., & Geels, C. (2013). The effect of climate and climate change on ammonia emissions in europe. *Atmospheric Chemistry and Physics*, *13*(1), 117–128. doi: 10.5194/acp-13-117-2013

Sommer, S. G., Webb, J., & Hutchings, N. D. (2019). New emission factors for calculation of ammonia volatilization from european livestock manure management systems. *Frontiers in Sustainable Food Systems*, *3*, 101. doi: 10.3389/fsufs.2019.00101

Stokstad, E. (2019). *Nitrogen crisis threatens Dutch environment—and economy.* American Association for the Advancement of Science. doi: 10.1126/science.366.6470.1180

Sun, K., Tao, L., Miller, D. J., Pan, D., Golston, L. M., Zondlo, M. A., ... Zhu, T. (2017). Vehicle Emissions as an Important Urban Ammonia Source in the United States and China. *Environ. Sci. Technol.*, *51*(4), 2472-2481. doi: 10.1021/acs.est.6b02805

Sutton, M. A., Asman, W. A., Ellermann, T., Van Jaarsveld, J., Acker, K., Aneja,

V., ... others   (2003).   Establishing the link between ammonia emission control and measurements of reduced nitrogen concentrations and deposition. *Environmental Monitoring and Assessment*, *82*(2), 149–185.   doi: 10.1023/A:1021834132138

Sutton, M. A., Burkhardt, J., Guerin, D., Nemitz, E., & Fowler, D. (1998). Development of resistance models to describe measurements of bi-directional ammonia surface–atmosphere exchange.   *Atmospheric Environment*, *32*(3), 473 - 480. doi: https://doi.org/10.1016/S1352-2310(97)00164-7

Sutton, M. A., Dragosits, U., Geels, C., Gyldenkærne, S., Misselbrook, T. H., & Bussink, W.   (2015).   Review on the scientific underpinning of calculation of ammonia emission and deposition in the netherlands.   *Wageningen University & Research*.

Sutton, M. A., Reis, S., Riddick, S. N., Dragosits, U., Nemitz, E., Theobald, M. R., ... de Vries, W.   (2013).   Towards a climate-dependent paradigm of ammonia emission and deposition.   *Philosophical Transactions of the Royal Society B: Biological Sciences*, *368*(1621), 20130166. doi: 10.1098/rstb.2013.0166

Sutton, M. A., van Dijk, N., Levy, P. E., Jones, M. R., Leith, I. D., Sheppard, L. J., ... Wolseley, P. A.   (2020).   Alkaline air: changing perspectives on nitrogen and air pollution in an ammonia-rich world.   *Philosophical Transactions of the Royal Society A: Mathematical, Physical and Engineering Sciences*, *378*(2183), 20190315. doi: 10.1098/rsta.2019.0315

Tang, Y. S., Braban, C. F., Dragosits, U., Dore, A. J., Simmons, I., van Dijk, N., ... Sutton, M. A.   (2018).   Drivers for spatial, temporal and long-term trends in atmospheric ammonia and ammonium in the uk.   *Atmospheric Chemistry and Physics*, *18*(2), 705–733. doi: 10.5194/acp-18-705-2018

Tang, Y. S., Flechard, C. R., Dämmgen, U., Vidic, S., Djuricic, V., Mitosinkova, M., ... Sutton, M. A.   (2021).   Pan-european rural monitoring network shows dominance of nh_3 gas and nh_4no_3 aerosol in inorganic atmospheric pollution load.   *Atmospheric Chemistry and Physics*, *21*(2), 875–914.   doi: 10.5194/acp-21-875-2021

Tang, Y. S., Stephens, A., Poskitt, J., Nemitz, E., Bealey, W. J., Leaver, D., ... Braban, C. F.   (2018).   UK Eutrophying and Acidifying Atmospheric Pollutant project's National Ammonia Monitoring Network (Data funded by Defra

and the Devolved Administrations and published under the Open Government Licence v3.0, NAMN, http://uk-air.defra.gov.uk/networks/network-info?view=ukeap).

Tobin, D. (2012). *Early Checkout of the Cross-track Infrared Sounder (CrIS) on Suomi-NPP, Through the Atmosphere, Summer 2012.*

Tørseth, K., Aas, W., Breivik, K., Fjæraa, A. M., Fiebig, M., Hjellbrekke, A. G., . . . Yttri, K. E. (2012). Introduction to the european monitoring and evaluation programme (emep) and observed atmospheric composition change during 1972ndash;2009. *Atmospheric Chemistry and Physics*, *12*(12), 5447–5481. doi: 10.5194/acp-12-5447-2012

Twigg, M. M., Di Marco, C. F., Leeson, S., van Dijk, N., Jones, M. R., Leith, I. D., . . . Cape, J. N. (2015). Water soluble aerosols and gases at a uk background site – part 1: Controls of $pm_{2.5}$ and pm_{10} aerosol composition. *Atmospheric Chemistry and Physics*, *15*(14), 8131–8145. doi: 10.5194/acp-15-8131-2015

UNECE. (1999). The 1999 Gothenburg Protocol to Abate Acidification, Eutrophication and Ground-level Ozone. Retrieved from `http://www.unece.org/env/lrtap/multi_h1.html`

U.S. EPA. (2018). Data from the 2014 National Emissions Inventory. , *Version2*.

van Zanten, M., Wichink Kruit, R., Hoogerbrugge, R., Van der Swaluw, E., & van Pul, W. (2017). Trends in ammonia measurements in the netherlands over the period 1993–2014. *Atmospheric Environment*, *148*, 352-360. doi: https://doi.org/10.1016/j.atmosenv.2016.11.007

Van Damme, M., Clarisse, L., Franco, B., Sutton, M. A., Erisman, J. W., Kruit, R. W., . . . Coheur, P.-F. (2020). Global, regional and national trends of atmospheric ammonia derived from a decadal (2008-2018) satellite record. *Environmental Research Letters*. Retrieved from `http://iopscience.iop.org/article/10.1088/1748-9326/abd5e0`

Van Damme, M., Clarisse, L., Heald, C. L., Hurtmans, D., Ngadi, Y., Clerbaux, C., . . . Coheur, P. F. (2014). Global distributions, time series and error characterization of atmospheric ammonia (NH_3) from IASI satellite observations. *Atmos. Chem. Phys.*, *14*(6), 2905–2922. doi: 10.5194/acp-14-2905-2014

Van Damme, M., Clarisse, L., Whitburn, S., Hadji-Lazaro, J., Hurtmans, D., Clerbaux, C., & Coheur, P.-F. (2018). Industrial and agricultural ammonia point

1195   sources exposed. *Nature*, *564*(7734), 99. doi: 10.1038/s41586-018-0747-1

1196 van der Graaf, S., Dammers, E., Segers, A., Kranenburg, R., Schaap, M., Shephard,

1197   M., & Erisman, J. W. (2021). Data assimilation of CrIS-NH3 satellite obser-

1198   vations for improving spatiotemporal NH_3 distributions in LOTOS-EUROS.

1199   *under review, Atmospheric Chemistry and Physics*.

1200 van der Werf, G. R., Randerson, J. T., Giglio, L., Collatz, G. J., Mu, M., Kasib-

1201   hatla, P. S., . . . van Leeuwen, T. T. (2010). Global fire emissions and the

1202   contribution of deforestation, savanna, forest, agricultural, and peat fires

1203   (1997–2009). *Atmospheric Chemistry and Physics*, *10*(23), 11707–11735.

1204   doi: 10.5194/acp-10-11707-2010

1205 von Bobrutzki, K., Braban, C. F., Famulari, D., Jones, S. K., Blackall, T., Smith,

1206   T. E. L., . . . Nemitz, E. (2010). Field inter-comparison of eleven atmospheric

1207   ammonia measurement techniques. *Atmospheric Measurement Techniques*,

1208   *3*(1), 91–112. doi: 10.5194/amt-3-91-2010

1209 Walker, H. L., Heal, M. R., Braban, C. F., Ritchie, S., Conolly, C., Sanocka, A.,

1210   . . . Twigg, M. M. (2019, may). Changing supersites: assessing the im-

1211   pact of the southern UK EMEP supersite relocation on measured atmo-

1212   spheric composition. *Environmental Research Communications*, *1*(4),

1213   041001. Retrieved from `https://doi.org/10.1088/2515-7620/ab1a6f` doi:

1214   10.1088/2515-7620/ab1a6f

1215 Walker, J. T., Jones, M. R., Bash, J. O., Myles, L., Meyers, T., Schwede, D.,

1216   . . . Robarge, W. (2013). Processes of ammonia air–surface exchange

1217   in a fertilized zea mays canopy. *Biogeosciences*, *10*(2), 981–998. Re-

1218   trieved from `https://bg.copernicus.org/articles/10/981/2013/` doi:

1219   10.5194/bg-10-981-2013

1220 Wang, Q., Jacob, D. J., Fisher, J. A., Mao, J., Leibensperger, E. M., Carouge, C. C.,

1221   . . . Doherty, S. J. (2011). Sources of carbonaceous aerosols and deposited

1222   black carbon in the Arctic in winter-spring: Implications for radiative forcing.

1223   *Atmos. Chem. Phys.*, *11*(23), 12453–12473. doi: 10.5194/acp-11-12453-2011

1224 Wang, R., Guo, X., Pan, D., Kelly, J. T., Bash, J. O., Sun, K., . . . Zondlo, M. A.

1225   (2021). Monthly patterns of ammonia over the contiguous united states at

1226   2-km resolution. *Geophysical Research Letters*, *48*(5), e2020GL090579. doi:

1227   https://doi.org/10.1029/2020GL090579

Wang, Y., Jacob, D. J., & Logan, J. A. (1998). Global simulation of tropospheric O_3-NO_x-hydrocarbon chemistry: 1. Model formulation. *J. Geophys. Res.*, *103*(D9), 10713-10725. doi: 10.1029/98JD00158

Warner, J. X., Dickerson, R. R., Wei, Z., Strow, L. L., Wang, Y., & Liang, Q. (2017). Increased atmospheric ammonia over the world's major agricultural areas detected from space. *Geophysical Research Letters*, *44*(6), 2875-2884. doi: 10.1002/2016GL072305

Warner, J. X., Wei, Z., Strow, L. L., Dickerson, R. R., & Nowak, J. B. (2016). The global tropospheric ammonia distribution as seen in the 13-year AIRS measurement record. *Atmos. Chem. Phys.*, *16*(8), 5467–5479. doi: 10.5194/acp-16-5467-2016

Wesely, M. (1989). Parameterization of surface resistances to gaseous dry deposition in regional-scale numerical models. *Atmos. Environ.*, *23*(6), 1293 - 1304. doi: 10.1016/0004-6981(89)90153-4

Whitehead, J., Longley, I., & Gallagher, M. (2007). Seasonal and diurnal variation in atmospheric ammonia in an urban environment measured using a quantum cascade laser absorption spectrometer. *Water, air, and soil pollution*, *183*(1), 317–329. doi: 10.1007/s11270-007-9381-5

Wichink Kruit, R. J., Schaap, M., Sauter, F. J., van Zanten, M. C., & van Pul, W. A. J. (2012). Modeling the distribution of ammonia across europe including bi-directional surface–atmosphere exchange. *Biogeosciences*, *9*(12), 5261–5277. doi: 10.5194/bg-9-5261-2012

Wintjen, P., Schrader, F., Schaap, M., Beudert, B., & Brümmer, C. (2020). Forest-atmosphere exchange of reactive nitrogen in a low polluted area – temporal dynamics and annual budgets. *Biogeosciences Discussions*, *2020*, 1–47. doi: 10.5194/bg-2020-364

Yu, F., Nair, A. A., & Luo, G. (2018). Long-term trend of gaseous ammonia over the United States: Modeling and comparison with observations. *J. Geophys. Res.*, *123*(15), 8315-8325. doi: 10.1029/2018JD028412

Zavyalov, V., Esplin, M., Scott, D., Esplin, B., Bingham, G., Hoffman, E., . . . Phillips, L. (2013). Noise performance of the CrIS instrument. *J. Geophys. Res.*, *118*(23), 13,108-13,120. doi: 10.1002/2013JD020457

Zhang, L., Chen, Y., Zhao, Y., Henze, D. K., Zhu, L., Song, Y., . . . Huang, B.

(2018). Agricultural ammonia emissions in China: Reconciling bottom-up and top-down estimates. *Atmos. Chem. Phys.*, *18*(1), 339–355. doi: 10.5194/acp-18-339-2018

Zhang, L., Gong, S., Padro, J., & Barrie, L. (2001). A size-segregated particle dry deposition scheme for an atmospheric aerosol module. *Atmos. Environ.*, *35*(3), 549 - 560. doi: 10.1016/S1352-2310(00)00326-5

Zhang, L., Jacob, D. J., Knipping, E. M., Kumar, N., Munger, J. W., Carouge, C. C., . . . Chen, D. (2012). Nitrogen deposition to the United States: Distribution, sources, and processes. *Atmos. Chem. Phys.*, *12*(10), 4539–4554. doi: 10.5194/acp-12-4539-2012

Zhang, L., Jacob, D. J., Liu, X., Logan, J. A., Chance, K., Eldering, A., & Bojkov, B. R. (2010). Intercomparison methods for satellite measurements of atmospheric composition: application to tropospheric ozone from TES and OMI. *Atmospheric Chemistry and Physics*, *10*(10), 4725–4739. Retrieved from https://acp.copernicus.org/articles/10/4725/2010/ doi: 10.5194/acp-10-4725-2010

Zhang, X., Gu, B., van Grinsven, H., Lam, S. K., Liang, X., Bai, M., & Chen, D. (2020). Societal benefits of halving agricultural ammonia emissions in china far exceed the abatement costs. *Nature communications*, *11*(1), 1–10. doi: 10.1038/s41467-020-18196-z

Zhu, L., Henze, D., Bash, J., Jeong, G.-R., Cady-Pereira, K., Shephard, M., . . . Capps, S. (2015). Global evaluation of ammonia bidirectional exchange and livestock diurnal variation schemes. *Atmospheric Chemistry and Physics*, *15*(22), 12823–12843. Retrieved from https://acp.copernicus.org/articles/15/12823/2015/ doi: 10.5194/acp-15-12823-2015

Zhu, L., Henze, D. K., Bash, J. O., Cady-Pereira, K. E., Shephard, M. W., Luo, M., & Capps, S. L. (2015). Sources and impacts of atmospheric nh 3: current understanding and frontiers for modeling, measurements, and remote sensing in north america. *Current Pollution Reports*, *1*(2), 95–116. doi: 10.1007/s40726-015-0010-4

Zhu, L., Henze, D. K., Cady-Pereira, K. E., Shephard, M. W., Luo, M., Pinder, R. W., . . . Jeong, G.-R. (2013). Constraining U.S. ammonia emissions using TES remote sensing observations and the GEOS-Chem adjoint model. *J.*

1294   *Geophys. Res.*, *118*(8), 3355-3368. doi: 10.1002/jgrd.50166

1295 Zöll, U., Brümmer, C., Schrader, F., Ammann, C., Ibrom, A., Flechard, C. R.,

1296   . . . Kutsch, W. L.   (2016).   Surface–atmosphere exchange of ammonia over

1297   peatland using qcl-based eddy-covariance measurements and inferential

1298   modeling.   *Atmospheric Chemistry and Physics*, *16*(17), 11283–11299.   doi:

1299   10.5194/acp-16-11283-2016

1300 Zöll, U., Lucas-Moffat, A. M., Wintjen, P., Schrader, F., Beudert, B., & Brümmer,

1301   C.   (2019).   Is the biosphere-atmosphere exchange of total reactive nitrogen

1302   above forest driven by the same factors as carbon dioxide? an analysis using

1303   artificial neural networks.   *Atmospheric Environment*, *206*, 108-118.   doi:

1304   https://doi.org/10.1016/j.atmosenv.2019.02.042

Table 1: Setup for inversion experiments

Inversion experiments	Dry deposition scheme	Posterior emissions
IE_bi	bi-directional	Posterior_bi
IE_uni	uni-directional	Posterior_uni
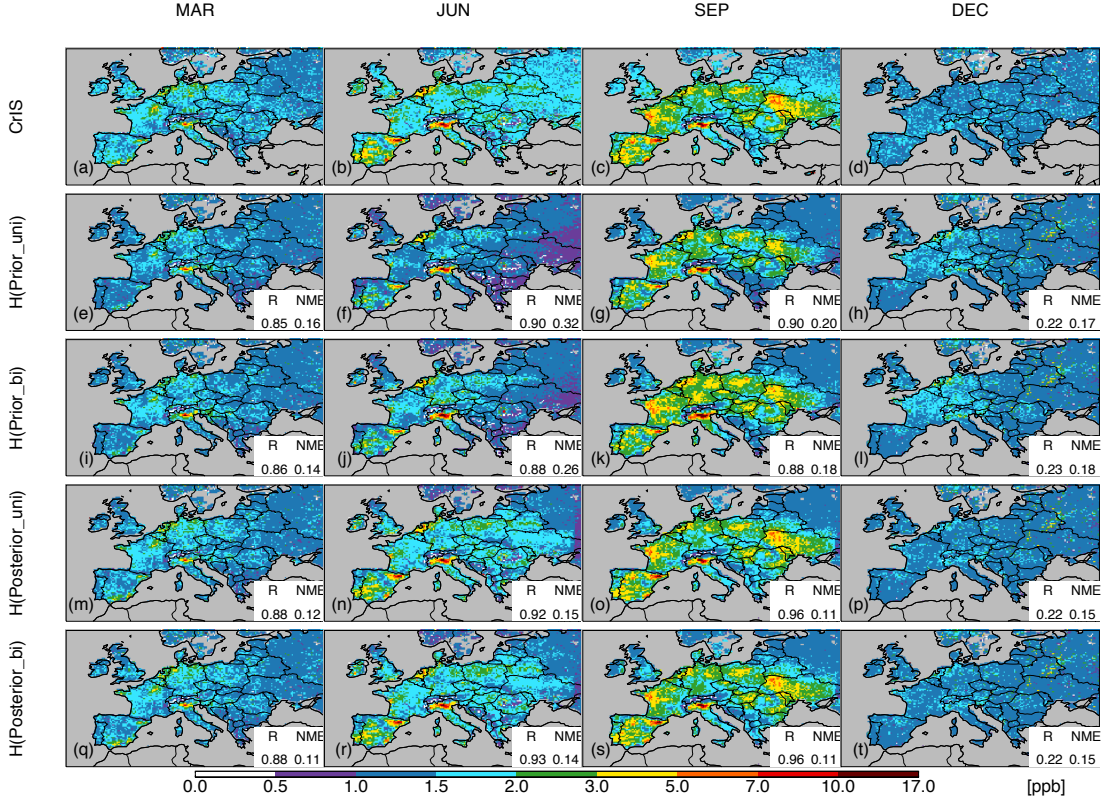
Figure 1: Monthly mean surface NH_3 concentrations from CrIS((a)-(d)), simulations driven by prior emissions with uni-di ((e)-(h)) and bi-di ((i)-(l)), simulations driven by posterior emissions derived through uni-di ((m)-(p)) and bi-di ((q)-(t)), respectively, in March, June, September and December in 2016. R is the spatial correlation coefficient between NH_3 simulation and CrIS surface NH_3; NME is the normalized mean error of NH_3 simulation relative to CrIS surface NH_3.
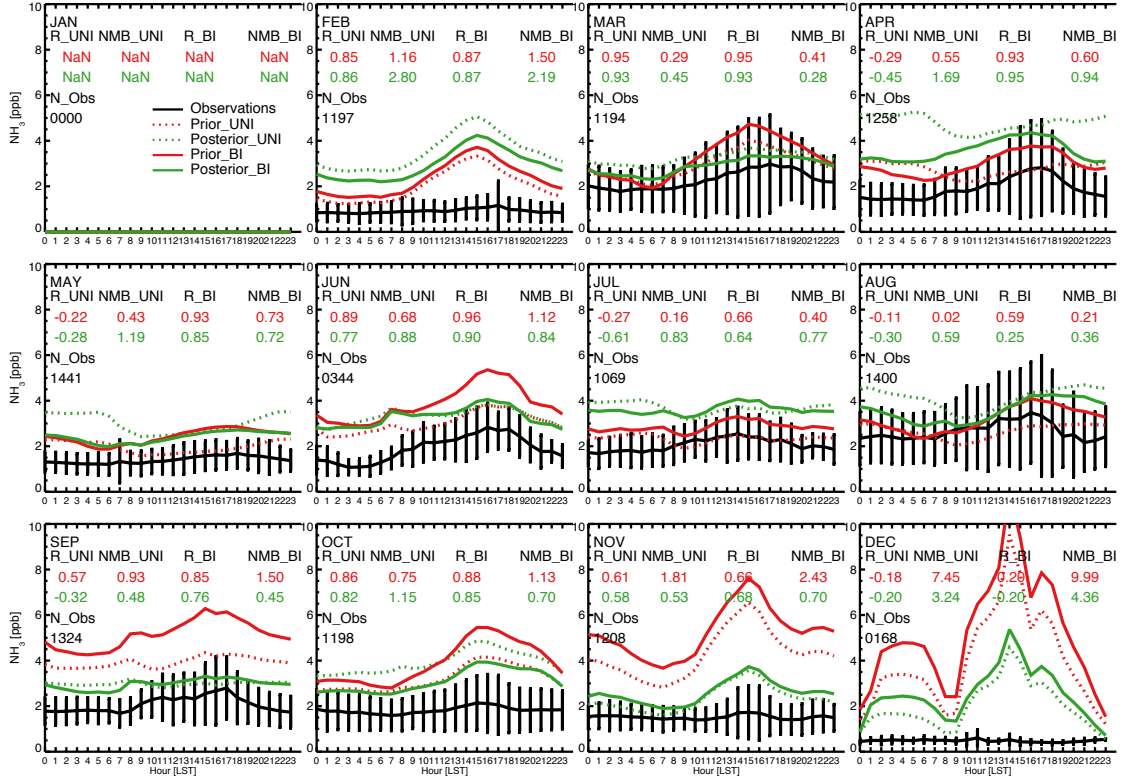
Figure 2: Monthly mean hourly surface NH$_3$ concentrations at a background site (Bavarian Forest National Park) [48°56$'$ N, 13°25$'$ E, 807 m a.s.l.] in Germany observed via QCL instrument (black) and simulated by GC driven by prior (red) and posterior (green) emissions through uni-di (dotted) and bi-di (solid) schemes for 11 months in 2016.
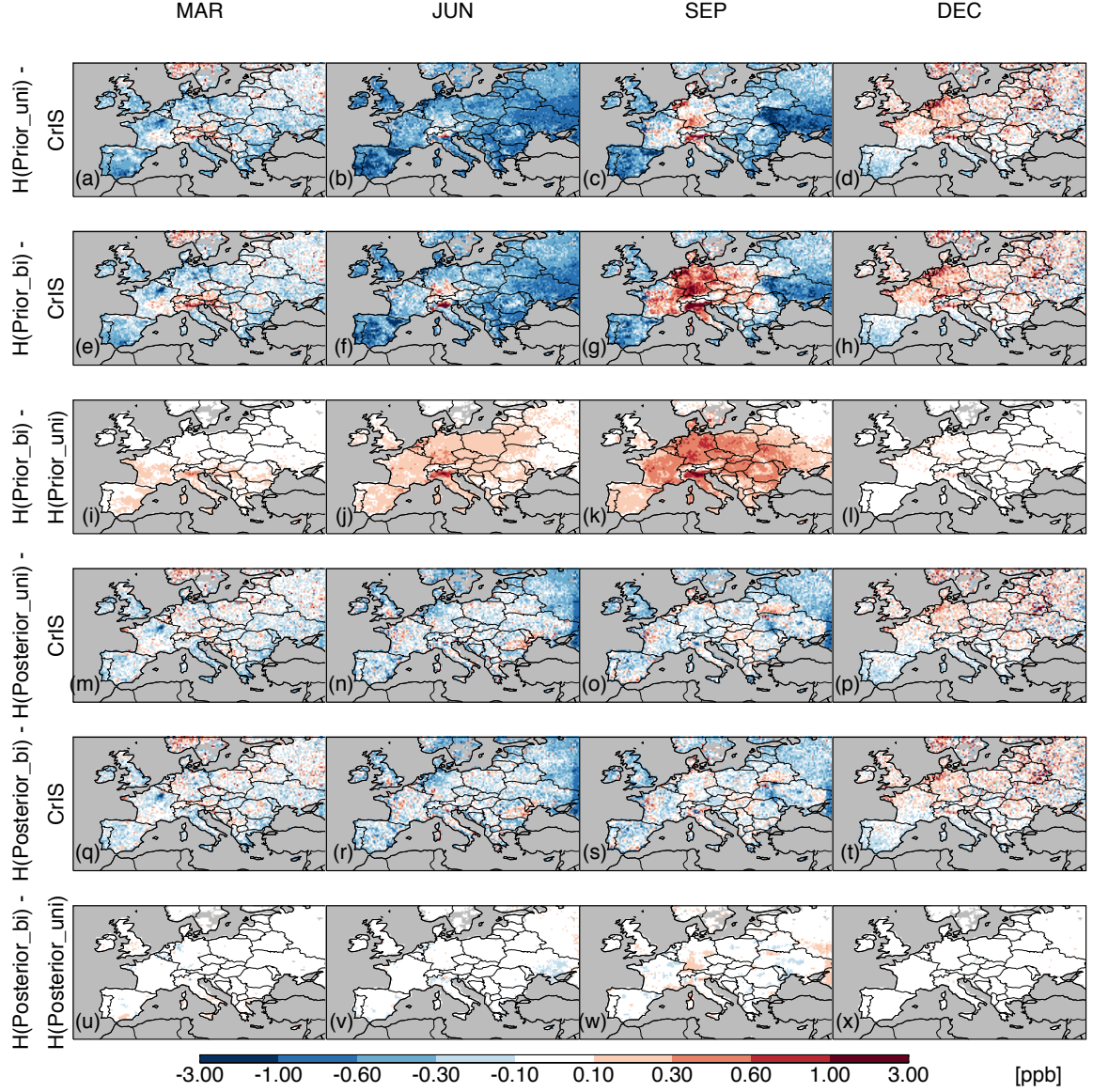
Figure 3: Difference between monthly mean CrIS surface NH$_3$ concentrations and prior and posterior simulations with uni-di and bi-di, respectively, in March, June, September and December in 2016.
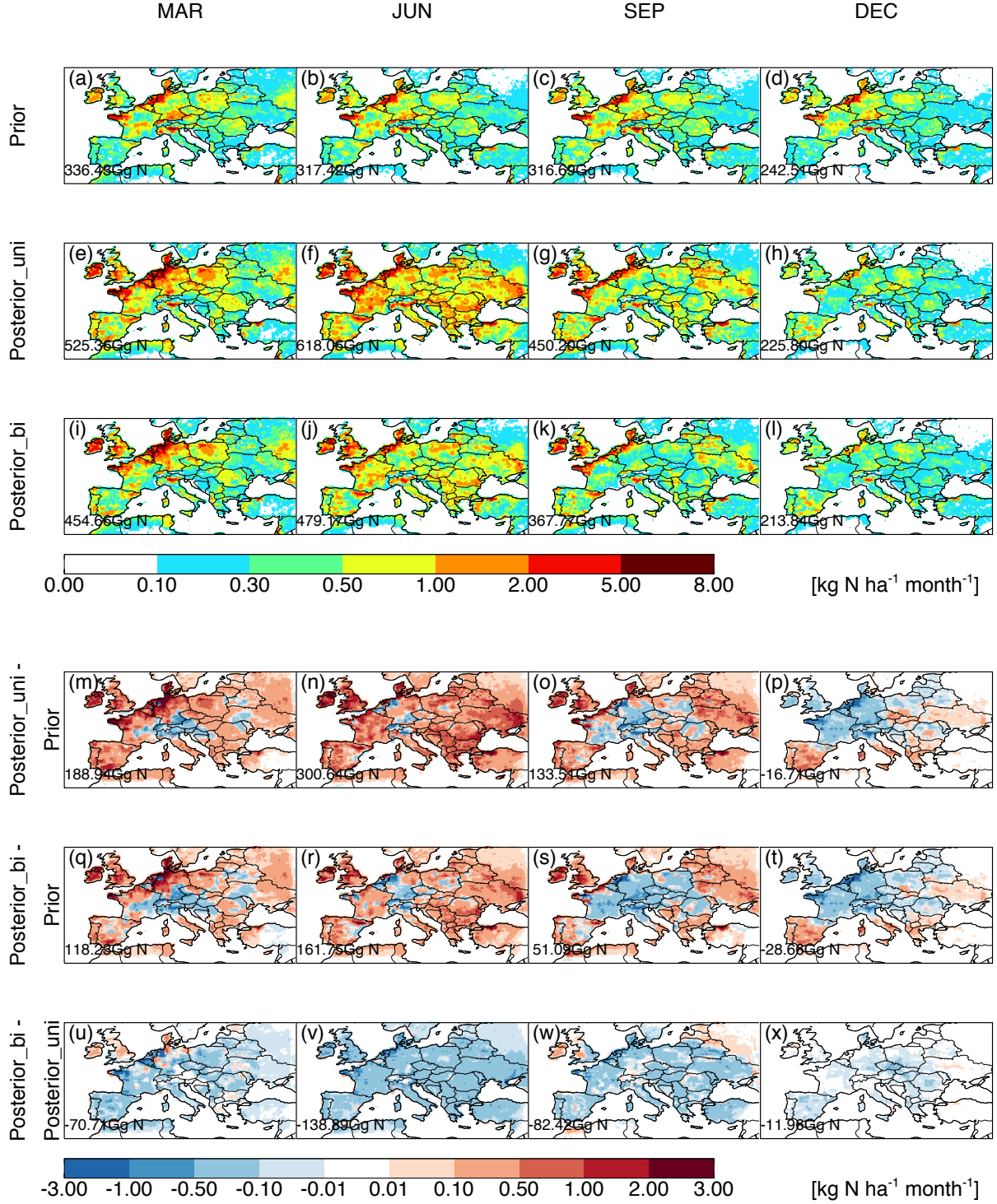
Figure 4: Spatial distribution of prior (first row), posterior (second and third row derived through uni-di and bi-di, respectively) monthly anthropogenic NH$_3$ emissions for March, June, September and December 2016 over Europe; difference (fourth and fifth row for uni-di and bi-di, respectivley) between posterior and prior monthly anthropogenic NH$_3$ emissions; difference (sixth row) between posterior monthly anthropogenic NH$_3$ emissions derived through uni-di and bi-di schemes.
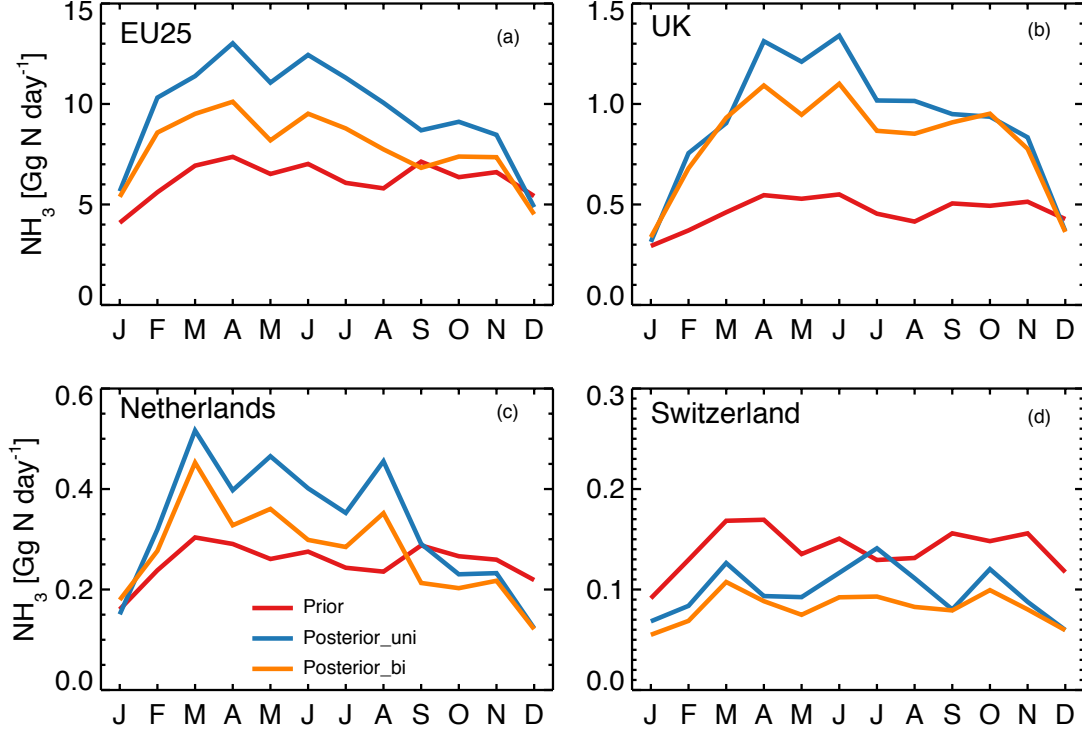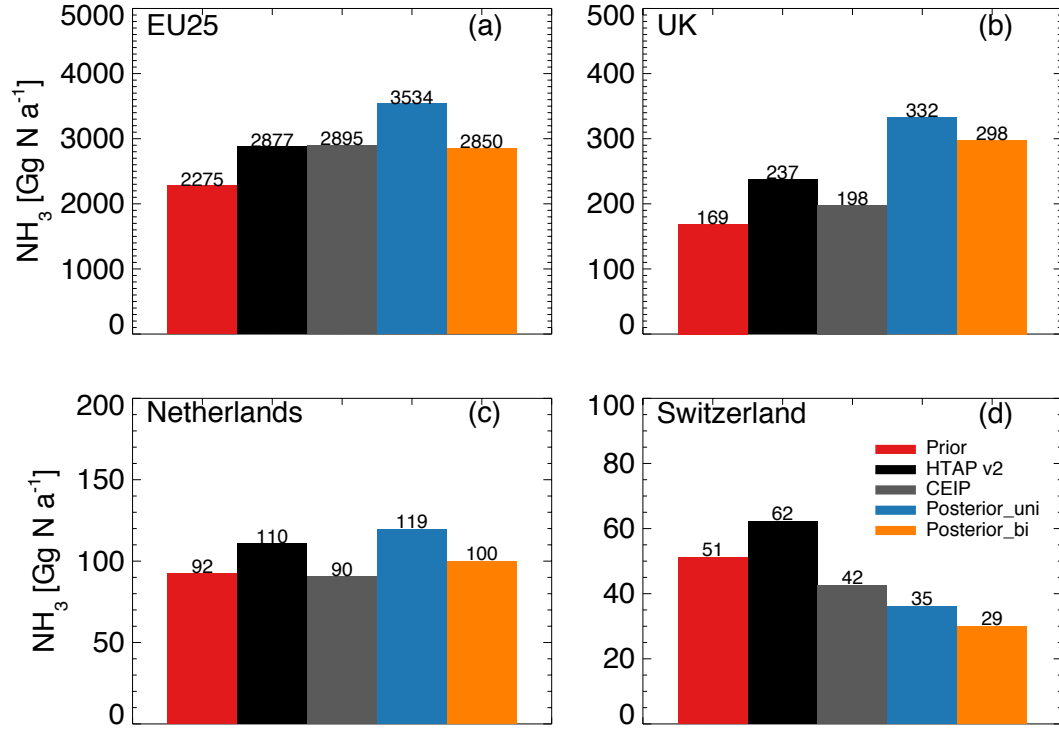
Figure 5: Regional/National monthly anthropogenic NH_3 emission estimates from prior inventory (red), and those derived from CrIS NH_3 with uni-directional scheme (blue) and with bi-directional scheme (orange), respectively. EU25 consists of Austria, Belgium, Bulgaria, Croatia, Republic of Cyprus, Czech Republic, Denmark, Estonia, France, Germany, Greece, Hungary, Ireland, Italy, Latvia, Lithuania, Luxembourg, Malta, Netherlands, Poland, Portugal, Romania, Slovakia, Slovenia and Spain.
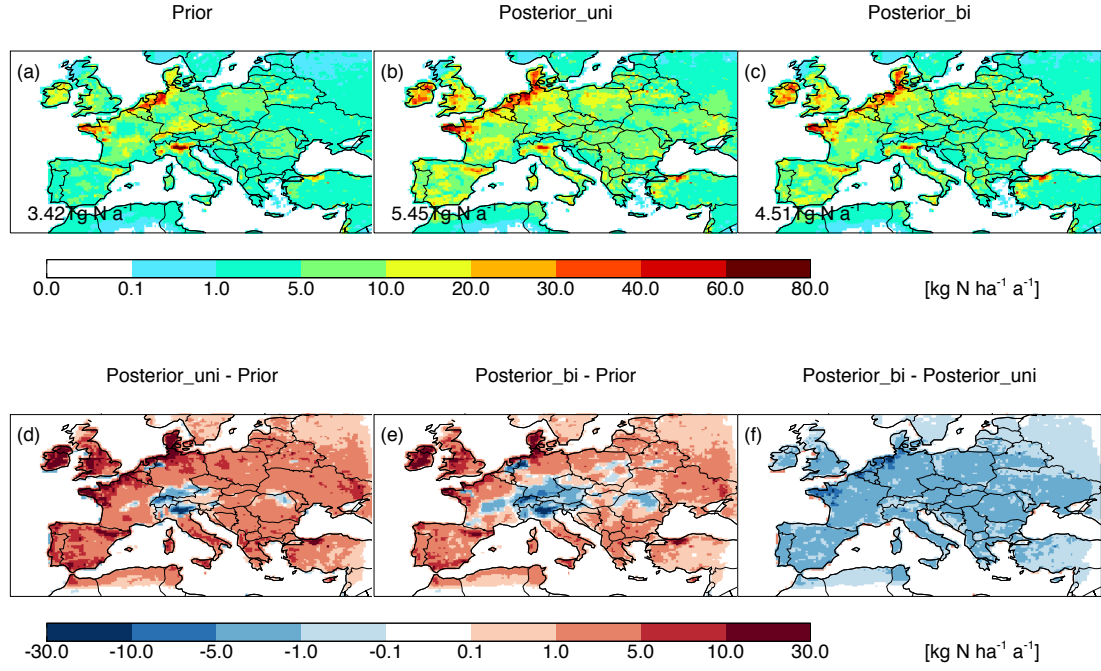
Figure 6: Spatial distribution of prior (a), posterior ((b) and (c) derived through uni-di and bi-di, respectively) annual anthropogenic NH_3 emissions over Europe in 2016; difference ((d) and (e) for uni-di and bi-di, respectivley) between posterior and prior annual anthropogenic NH_3 emissions; difference (f) between posterior annual anthropogenic NH_3 emissions derived through uni-di and bi-di schemes.

Figure 7: Regional/National total annual anthropogenic NH_3 emission estimates from prior inventory (red), HTAP v2 inventory (black, for 2010), CEIP inventory (gray, for 2016), and those derived from CrIS NH_3 through uni-di scheme (blue) and bi-di scheme (orange), respectively.
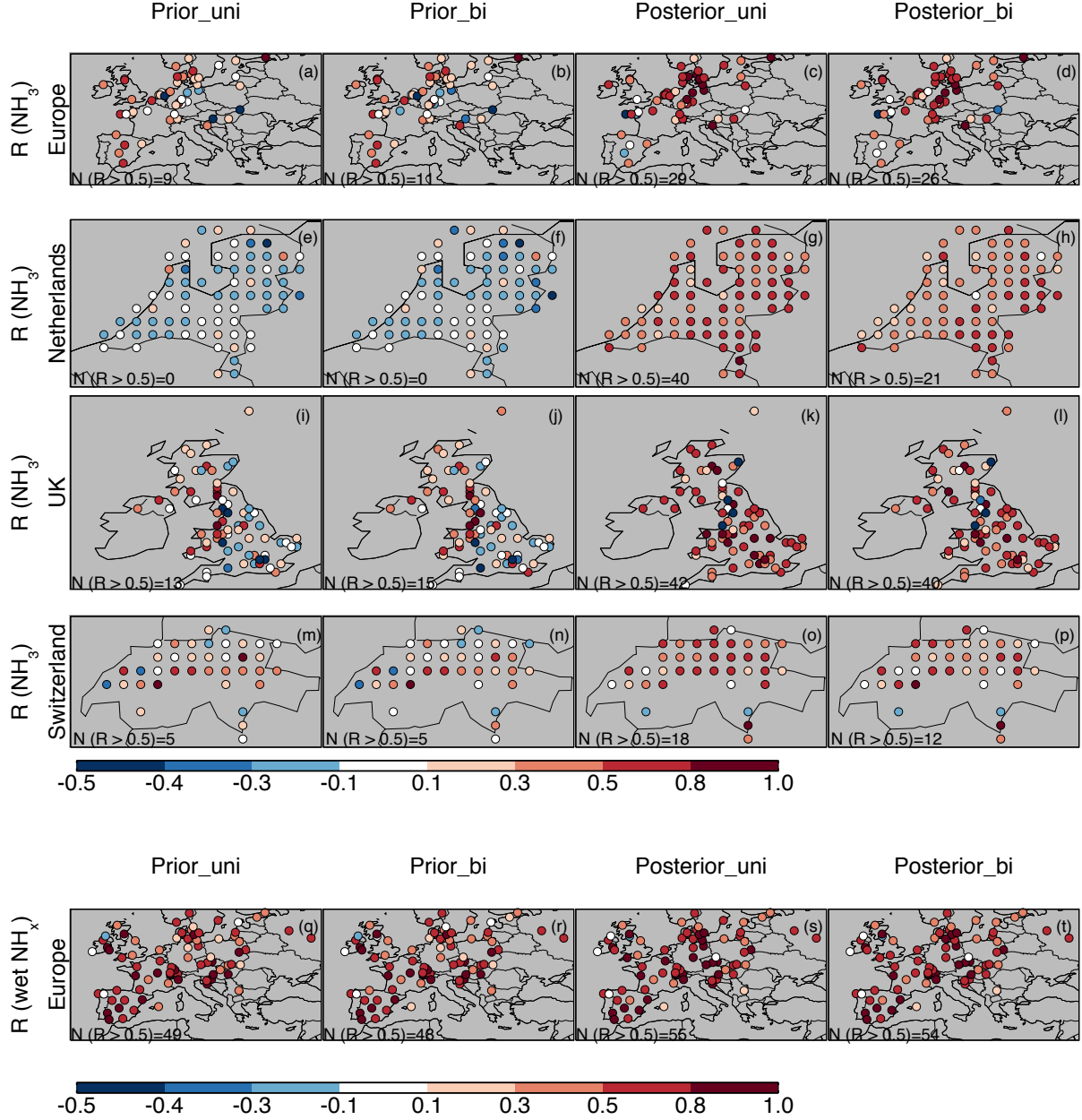
Figure 8: R between monthly mean surface NH_3 observations from European sites in 2016 (over Europe (a-d), Netherlands (e-h), UK (i-l) and Switzerland (m-p)) and simulations driven by prior and posterior emissions derived through uni-di and bi-di schemes, respectively, with linear averaging kernel. R between monthly mean NH_x wet deposition measurements and simulations over Europe (q-t) in 2016.
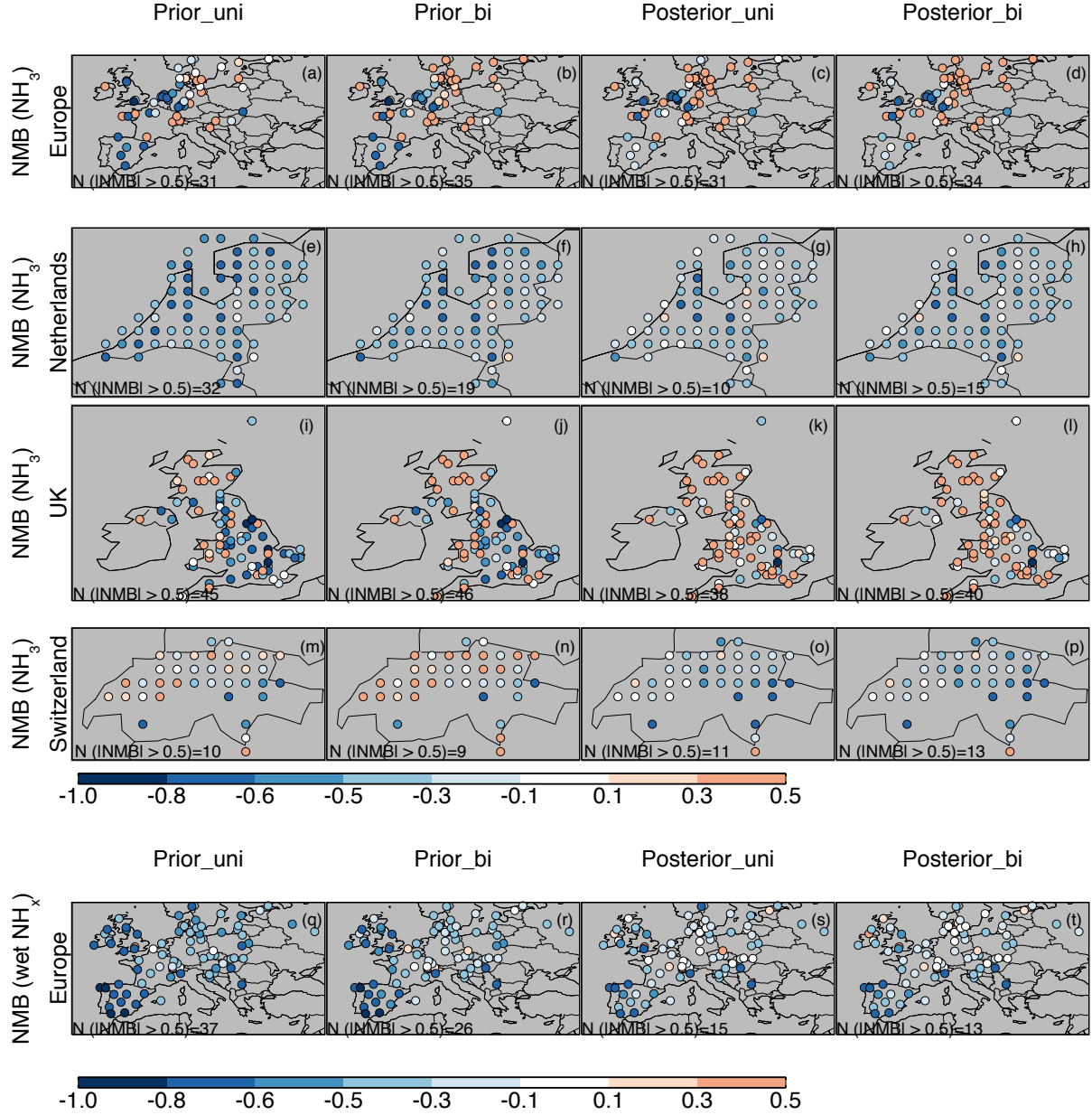
Figure 9: Annual NMB of monthly surface NH$_3$ simulations driven by prior and posterior emissions relative to monthly mean surface NH$_3$ observations from many sites in 2016 over Europe (a-d), Netherlands (e-h), UK (i-l) and Switzerland (m-p). Annual NMB of monthly NH$_x$ wet deposition simulations relative to monthly mean NH$_x$ wet deposition measurements over Europe (q-t) in 2016.
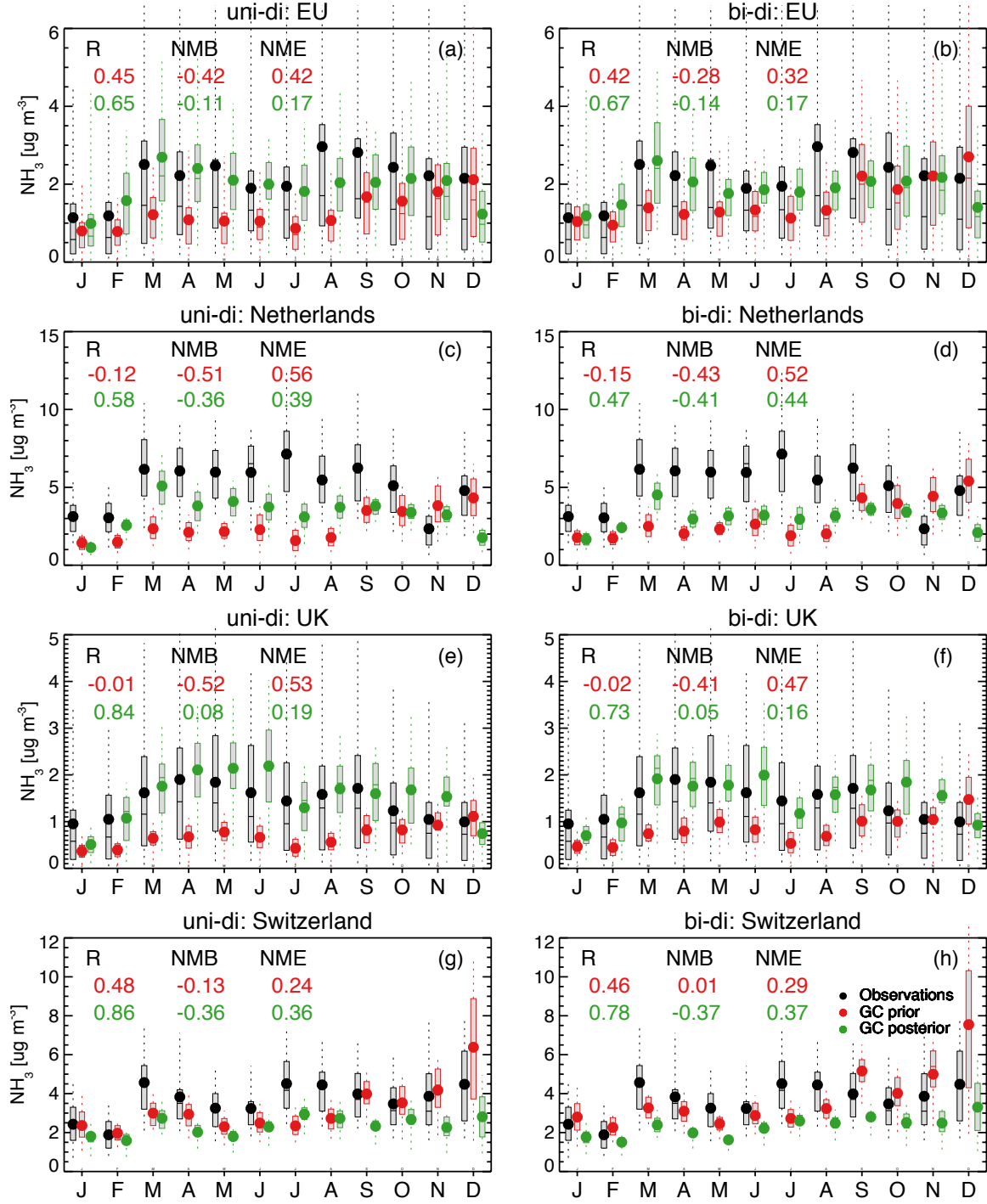
Figure 10: Comparison between domain-averaged monthly mean surface NH₃ observations (black) from European sites in 2016 and simulations driven by prior (red) and posterior (green) emissions derived through uni-di and bi-di schemes, respectively.
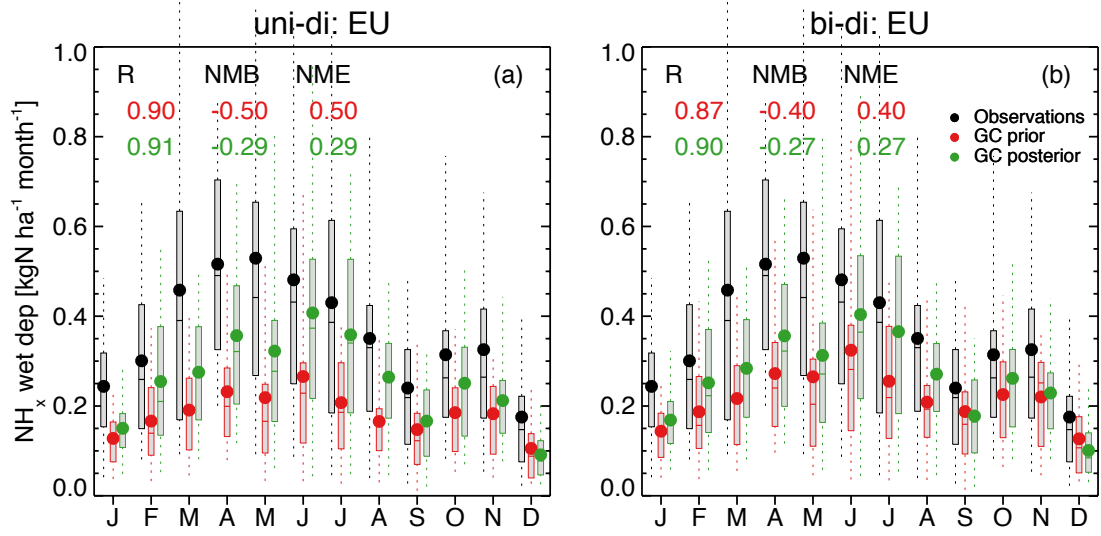
Figure 11: Comparison between domain-averaged monthly mean NH_x wet deposition observations (black) from European (EMEP) sites in 2016 and simulations driven by prior (red) and posterior (green) emissions derived through uni-di and bi-di schemes, respectively.

Supporting Information for
"4D-Var inversion of European NH₃ emissions using CrIS NH₃ measurements and GEOS-Chem adjoint with bi-directional and uni-directional flux schemes"

Hansen Cao[1], Daven K. Henze[1], Liye Zhu[2], Mark W. Shephard[3], Karen Cady-Pereira[4], Enrico Dammers[5], Michael Sitwell[3], Nicholas Heath[4], Chantelle Lonsdale[6], Jesse O. Bash[7], Kazuyuki Miyazaki [8], Christophe Flechard[9], Yannick Fauvel[9], Roy Wichink Kruit[10], Stefan Feigenspan[11], Christian Brümmer[12], Frederik Schrader[12], Marsailidh M. Twigg[13], Sarah Leeson[13], Yuk S. Tang[13], Amy C.M. Stephens[13], Christine Braban[13], Keith Vincent[14], Mario Meier[15], Eva Seitler[15], Camilla Geels[16], Thomas Ellermann[16], Agnieszka Sanocka[14], Shannon L. Capps[17]

[1]University of Colorado, Boulder, USA
[2]Sun Yat-sen University, China
[3]Environment and Climate Change Canada, Toronto, Ontario, Canada
[4]Atmospheric and Environmental Research Inc., USA
[5]Netherlands Organisation for Applied Scientific Research (TNO), Climate Air and Sustainability (CAS), Utrecht, The Netherlands
[6]Department of Civil, Structural and Environmental Engineering, University at Buffalo, Buffalo, NY USA
[7]U.S. Environmental Protection Agency, USA
[8]Jet Propulsion Laboratory, California Institute of Technology, USA
[9]INRAE (National Research Institute for Agriculture, Food and Environment), UMR SAS, Agrocampus Ouest, 65 rue de Saint-Brieuc, 35042 Rennes, France
[10]National Institute for Public Health and the Environment, The Netherlands
[11]German Environment Agency, Germany
[12]Thünen Institute of Climate-Smart Agriculture, Germany
[13]UK Centre for Ecology & Hydrology, UK
[14]Ricardo Energy & Environment, Wantage, England, UK
[15]Forschungsstelle für Umweltbeobachtung, Switzerland
[16]Department of Environmental Science, Aarhus University, Denmark
[17]Civil, Architectural, and Environmental Engineering Department, Drexel University, Philadelphia, PA, USA

Contents

Supporting figures and tables

Corresponding author: Daven K. Henze, `daven.henze@colorado.edu`
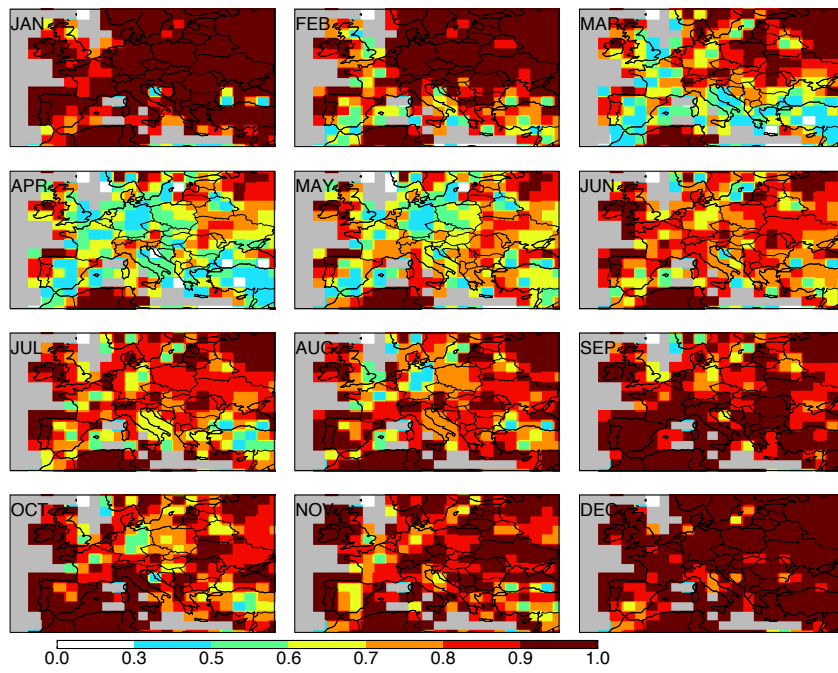
Figure S1: MASAGE-based ratio of monthly livestock NH_3 emissions to monthly total anthropogenic NH_3 emissions.
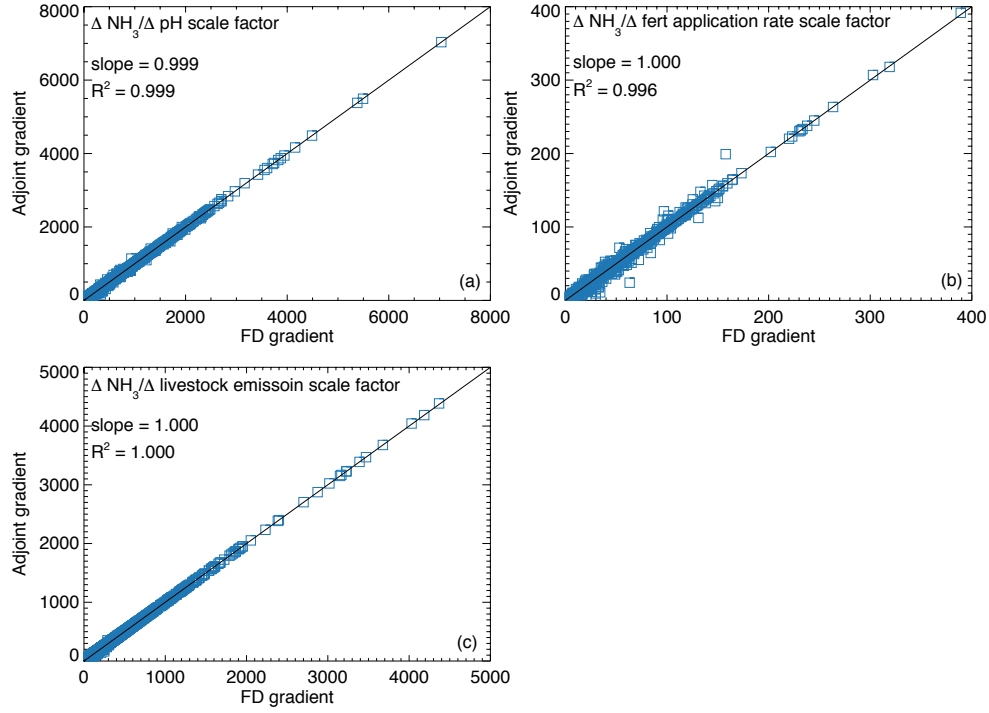
Figure S2: Scatter plot between adjoint gradient and finite difference (FD) gradient of simulated NH3 with respect to pH scale factor (a), fertilizer application rate scale factor (b) and livestock emission scale factor (c), respectively, from July 1st to 7th 2016 for the Europe domain at $0.3125^{o} \times 0.25^{o}$.